

**SYNTHESIS, CHARACTERIZATION AND  
BIOLOGICAL PROPERTIES OF NICKEL- AND IRON-  
CARBOXYLATE COMPLEXES**

**CH'NG CYNN DEE**

**UNIVERSITI SAINS MALAYSIA**

**2010**

**SYNTHESIS, CHARACTERIZATION AND  
BIOLOGICAL PROPERTIES OF NICKEL- AND IRON-  
CARBOXYLATE COMPLEXES**

**by**

**CH'NG CYNN DEE**

**Thesis submitted in fulfillment of the requirement  
For the degree of  
Master of Science**

**August 2010**

## ACKNOWLEDGEMENT

First and foremost, I would like to thank and acknowledge my supervisor, Prof. Teoh Siang Guan for giving me opportunity to learn under his guidance. His professionalism, helpful guidance and support have made this research a success.

Nevertheless, I would like to acknowledge Prof. Fun Hoong Kun of School of Physics, USM for his help and advice in single crystal X-ray structural determination. I am also thankful to Dr. Tang Thean Hock of Advanced Medical and Dental Institute, USM for his help in DNA cleavage experiment and Dr. Alexander Chong Shu Chien of School of Biological Sciences, USM for his help in cytotoxic assay.

Next, I would like to express my thanks to all the laboratory assistants, Mr. Aw Yeong Cheok Hoe (FTIR Analysis), Mr. Ong Chin Hin, Mr. Razly Effendy (CHN Analysis), Mr. Marimuthu (AAS Analysis) and Mr. Burhanuddin Saad (TGA) for being so patience and lending me a helping hand each time experiments are conducted. I also like to thank my seniors, Mr. Lim Eng Khoon and Mr. William for their guidance, support and encouragement.

Apart from this, I wish to express my greatest appreciation to my parents for their moral support and encouragement throughout my candidature.

Last but not least, I would like to extend my appreciation to those who have given me a helping hand, advice and guidance directly and indirectly during the period of my study.

## TABLES OF CONTENTS

	Page
Acknowledgement	ii
Tables of Contents	iii
List of Tables	viii
List of Figures	xi
List of Abbreviations	xxii
Abstrak	xxiv
Abstract	xxvi
<b>CHAPTER 1 – INTRODUCTION</b>	
1.1 Nickel	1
1.1.1 Applications of Nickel	1
1.2 Iron	2
1.2.1 Applications of Iron	2
1.3 Transition Metal Complexes	3
1.4 DNA	4
1.5 The Interaction Of Transition Metal Complexes and DNA	6
1.6 Transition Metal Complexes as Anticancer Agents	8
1.7 Mechanism of DNA Cleavage	9
1.8 Biological Activity of Nickel(II) Complexes	11
1.9 Biological Activity of Iron Complexes	14
1.10 Objectives and Scope of Study	18

## **CHAPTER 2 - MATERIALS AND METHODS**

2.1	Reagents	20
2.2	Instrumentation	21
2.3	Experimental	22
2.4	Methods of Characterization	
2.4.1	Determination of the melting point of complexes	22
2.4.2	Conductivity Measurement	23
2.4.3	Analysis of Fourier Transform Infrared Spectroscopy (FT-IR)	23
2.4.4	CHN Microanalysis	23
2.4.5	Analysis of Atomic Absorption Spectrometry (AAS)	23
2.4.6	Analysis of Ultraviolet-Visible (UV-Vis) Spectrometry	25
2.4.7	Analysis of Cyclic Voltammetry (CV)	26
2.4.8	Analysis of Thermogravimetric Analysis (TGA)	26
2.4.9	X-Ray Crystallography	26
2.4.10	DNA Cleavage Experiments	27
2.4.11	Cytotoxic Assay	27

## **CHAPTER 3 - RESULT AND DISCUSSION**

3.1	Characterization of Ni(gly), Ni(ala) and Ni(his) complexes	
3.1.1	Determination of yield and physical properties	30
3.1.2	Conductivity Measurement	35
3.1.3	Analysis of Fourier Transform Infrared Spectroscopy (FT-IR)	35
3.1.4	CHN Microanalysis	39
3.1.5	Analysis of Atomic Absorption Spectroscopy (AAS)	40
3.1.6	Analysis of Ultraviolet-Visible Spectrometry	41

3.1.7	Analysis of Cyclic Voltammetry (CV)	42
3.1.8	Analysis of Thermogravimetric Analysis (TGA)	45
3.1.9	X-Ray Crystallography and Structure	52
3.1.10	DNA Cleavage Experiments	60
3.1.11	Cytotoxic Assay	65
3.2	Characterization of Ni(2-pic), Ni(3,5-dinitro) and Ni(4-amino) complexes	
3.2.1	Determination of yield and physical properties	67
3.2.2	Conductivity Measurement	71
3.2.3	Analysis of Fourier Transform Infrared Spectroscopy (FT-IR)	72
3.2.4	CHN Microanalysis	75
3.2.5	Analysis of Atomic Absorption Spectroscopy (AAS)	76
3.2.6	Analysis of Ultraviolet-Visible Spectrometry	77
3.2.7	Analysis of Cyclic Voltammetry (CV)	78
3.2.8	Analysis of Thermogravimetric Analysis (TGA)	81
3.2.9	X-Ray Crystallography and Structure	88
3.2.10	DNA Cleavage Experiments	90
3.2.11	Cytotoxic Assay	94
3.3	Characterization of Ni(pyr) and Fe(pyr) complexes	
3.3.1	Determination of yield and physical properties	96
3.3.2	Conductivity Measurement	98
3.3.3	Analysis of Fourier Transform Infrared Spectroscopy (FT-IR)	99
3.3.4	CHN Microanalysis	101
3.3.5	Analysis of Atomic Absorption Spectroscopy (AAS)	101

3.3.6	Analysis of Ultraviolet-Visible Spectrometry	102
3.3.7	Analysis of Cyclic Voltammetry (CV)	104
3.3.8	Analysis of Thermogravimetric Analysis (TGA)	106
3.3.9	X-Ray Crystallography and Structure	110
3.3.10	DNA Cleavage Experiments	112
3.3.11	Cytotoxic Assay	115
3.4	Characterization of Ni(mal) and Fe(mal) complexes	
3.4.1	Determination of yield and physical properties	117
3.4.2	Conductivity Measurement	119
3.4.3	Analysis of Fourier Transform Infrared Spectroscopy (FT-IR)	120
3.4.4	CHN Microanalysis	122
3.4.5	Analysis of Atomic Absorption Spectroscopy (AAS)	122
3.4.6	Analysis of Ultraviolet-Visible Spectrometry	123
3.4.7	Analysis of Cyclic Voltammetry (CV)	125
3.4.8	Analysis of Thermogravimetric Analysis (TGA)	127
3.4.9	X-Ray Crystallography and Structure	131
3.4.10	DNA Cleavage Experiments	133
3.4.11	Cytotoxic Assay	136
3.5	Characterization of Ni(pdc) and Fe(pdc) complexes	
3.5.1	Determination of yield and physical properties	138
3.5.2	Conductivity Measurement	141
3.5.3	Analysis of Fourier Transform Infrared Spectroscopy (FT-IR)	142
3.5.4	CHN Microanalysis	144

3.5.5	Analysis of Atomic Absorption Spectroscopy (AAS)	144
3.5.6	Analysis of Ultraviolet-Visible Spectrometry	145
3.5.7	Analysis of Cyclic Voltammetry (CV)	147
3.5.8	Analysis of Thermogravimetric Analysis (TGA)	149
3.5.9	X-Ray Crystallography and Structure	153
3.5.10	DNA Cleavage Experiments	155
3.5.11	Cytotoxic Assay	158
<b>CHAPTER 4 – CONCLUSION</b>		160
<b>REFERENCES</b>		162
<b>APPENDICES</b>		



## LIST OF TABLES

	Page	
Table 1.1	Selected IC <sub>50</sub> (μM) values assessed by a calcein AM assay	18
Table 1.2	Carboxylic acids utilised in this study	18
Table 2.1	Chemicals used in this research	20
Table 2.2	Biochemicals used in biology part	21
Table 2.3	Instruments used for the quantitative and qualitative characterizations	21
Table 3.1	The yield of each amino acid complex	34
Table 3.2	The physical properties of amino acid of nickel complexes	34
Table 3.3	The conductivity of amino acid of nickel complexes	35
Table 3.4	Molar conductance, $\Lambda$ of electrolyte solution which has 2, 3, 4 and 5 ions at 25 °C	35
Table 3.5	Selected infrared data of ligands, salts and complexes	39
Table 3.6	Percentage of C, H and N for Complexes Ni(gly), Ni(ala) and Ni(his)	39
Table 3.7	Percentage of Nickel for complexes Ni(gly), Ni(ala) and Ni(his)	40
Table 3.8	Thermogravimetric results of Ni(gly)	46
Table 3.9	Thermogravimetric results of Ni(ala)	49
Table 3.10	Thermogravimetric results of Ni(his)	51
Table 3.11	Crystallography data for Ni(gly)	57
Table 3.12	Geometry parameter, bond lengths (Å) and angles (°) for Ni(gly)	57
Table 3.13	Hydrogen bond geometry (Å, °) for Ni(gly)	58
Table 3.14	IC <sub>50</sub> values for Ni(gly), Ni(ala) and Ni(his) on HepG2	66
Table 3.15	The yield of each carboxylic acid complex	70
Table 3.16	The physical properties of carboxylic acid nickel complexes	71

Table 3.17	The conductivity of carboxylic acid of nickel complexes	71
Table 3.18	Selected infrared data of ligands, salts and complexes	75
Table 3.19	Percentage of C, H and N for complexes Ni(2-pic), Ni(3,5-dinitro) and Ni(4-amino)	75
Table 3.20	Percentage of Nickel for complexes Ni(2-pic), Ni(3,5-dinitro) and Ni(4-amino)	76
Table 3.21	Thermogravimetric results of Ni(2-Pic)	82
Table 3.22	Thermogravimetric results of Ni(3,5-dinitro)	84
Table 3.23	Thermogravimetric results of Ni(4-amino)	87
Table 3.24	IC <sub>50</sub> values for Ni(2-pic), Ni(3,5-dinitro) and Ni(4-amino) on HepG2	95
Table 3.25	The yield of Ni(pyr) and Fe(pyr) complexes	97
Table 3.26	The physical properties of Ni(pyr) and Fe(pyr) complexes	98
Table 3.27	The conductivity of Ni(pyr) and Fe(pyr) complexes	98
Table 3.28	Selected infrared data of ligands, salts and complexes	101
Table 3.29	Percentage of C, H and N for complexes Ni(pyr) and Fe(pyr)	101
Table 3.30	Percentage of complexes Ni(pyr) and Fe(pyr)	102
Table 3.31	Thermogravimetric results of Ni(pyr)	107
Table 3.32	Thermogravimetric results of Fe(pyr)	109
Table 3.33	IC <sub>50</sub> values for Ni(pyr) and Fe(pyr) on HepG2	116
Table 3.34	The yield of Ni(mal) and Fe(mal) complexes	118
Table 3.35	The physical properties of Ni(mal) and Fe(mal) complexes	119
Table 3.36	The conductivity of Ni(mal) and Fe(mal) complexes	119
Table 3.37	Selected infrared data of ligands, salts and complexes	122
Table 3.38	Percentage of C, H and N for complexes Ni(mal) and Fe(mal)	122
Table 3.39	Percentage of complexes Ni(mal) and Fe(mal)	123
Table 3.40	Thermogravimetric results of Ni(mal)	128

Table 3.41	Thermogravimetric results of Fe(mal)	130
Table 3.42	IC <sub>50</sub> values for Ni(mal) and Fe(mal) on HepG2	137
Table 3.43	The yield of Ni(pdc) and Fe(pdc) complexes	140
Table 3.44	The physical properties of Ni(pdc) and Fe(pdc) complexes	141
Table 3.45	The conductivity of Ni(pdc) and Fe(pdc) complexes	141
Table 3.46	Selected infrared data of ligands, salts and complexes	144
Table 3.47	Percentage of C, H and N for complexes Ni(pdc) and Fe(pdc)	144
Table 3.48	Percentage of complexes Ni(pdc) and Fe(pdc)	145
Table 3.49	Thermogravimetric results of Ni(pdc)	150
Table 3.50	Thermogravimetric results of Fe(pdc)	152
Table 3.51	IC <sub>50</sub> values for Ni(pdc) and Fe(pdc) on HepG2	159

## LIST OF FIGURES

		Page
Figure 1.1	Metals in biological systems: nickel in factor F430	2
Figure 1.2	Metals in biological systems: iron in heme, which is found in hemoglobin	3
Figure 1.3	(A) The structure of part of a DNA double helix (B) The chemical structure of DNA ( <a href="http://schools-wikipedia.org/wp/d/DNA.htm">http://schools-wikipedia.org/wp/d/DNA.htm</a> )	5
Figure 1.4	Three forms of DNA that can be tracked using agarous gel electrophoresis	8
Figure 1.5	Structural formula of cisplatin	9
Figure 1.6	Cisplatin analogues used in the clinic	9
Figure 1.7	Mechanism of Fenton reaction (X represents metal)	10
Figure 1.8	Schematic representation for the reaction of guanine with hydroxyl radicals	11
Figure 1.9	The structures of $[\text{NiCR}]^{2+}$ and $[\text{Ni}(\text{CR}-2\text{H})]^{2+}$ (Matkar <i>et al.</i> , 2006)	12
Figure 1.10	$[\text{NiCR}]^{2+}$ and $[\text{Ni}(\text{CR}-2\text{H})]^{2+}$ caused double-stranded DNA damage in vitro in the presence of oxone. The gel shows the DNA samples after piperidine treatment. Lane 1, linearized plasmid DNA treated with $[\text{NiCR}]^{2+}$ and oxone; lane 2, DNA treated with $[\text{Ni}(\text{CR}-2\text{H})]^{2+}$ and oxone; lane 3, DNA treated with oxone; lane 4, untreated control; M, marker (PstI-cut lambda DNA) (Matkar <i>et al.</i> , 2006)	13
Figure 1.11	Cytotoxicity of $[\text{Ni}(\text{CR}-2\text{H})]^{2+}$ . MCF-7 human breast cancer cells were treated with 10, 25, 50, 100 or 200 $\mu\text{M}$ $\text{NiCl}_2$ , $[\text{NiCR}]^{2+}$ or $[\text{Ni}(\text{CR}-2\text{H})]^{2+}$ and cell viability was determined by MTS assay. Diamonds ( $\blacklozenge$ ) stand for $[\text{Ni}(\text{CR}-2\text{H})]^{2+}$ , squares ( $\blacksquare$ ) for $[\text{NiCR}]^{2+}$ , and triangles ( $\blacktriangle$ ) for $\text{NiCl}_2$ (Matkar <i>et al.</i> , 2006).	13
Figure 1.12	Cytotoxic effects of NQTS and NQSC and their nickel(II) complexes on MCF-7 human breast cancer cells (Afrasiabi <i>et al.</i> , 2005)	14
Figure 1.13	ORTEP drawing of the $[\text{Fe}(\text{3hf})_2\text{Cl}(\text{MeOH})]$ complex (El Amrani <i>et al.</i> , 2006)	16

Figure 1.14	Agarose gel electrophoresis of pUC18 plasmid DNA treated with complex, FeCl <sub>3</sub> , and a mixture FeCl <sub>3</sub> + H3hf (1:2) in the presence of the 1 equiv ascorbate/H <sub>2</sub> O <sub>2</sub> . Lane 1: λDNA/EcoR1 + HindIII Marker; lane 2: supercoiled DNA; lane 3: supercoiled DNA + ascorbate/H <sub>2</sub> O <sub>2</sub> ; lane 4: 15 μM FeCl <sub>3</sub> ; lane 5: 21 μM FeCl <sub>3</sub> ; lane 6: 27 μM FeCl <sub>3</sub> ; lane 7: 27 μM FeCl <sub>3</sub> + 54 μM H3hf; lane 8: 15 μM complex; lane 9: 18 μM complex; lane 10: 21 μM complex; lane 11: 23 μM complex; lane 12: 25 μM complex; lane 13: 26 μM complex; lane 14: 27 μM complex; lane 15: 30 μM complex (El Amrani <i>et al.</i> , 2006)	17
Figure 2.1	The AAS calibration curve for nickel	24
Figure 2.2	The AAS calibration curve for iron	25
Figure 2.3	The AAS calibration curve for potassium	25
Figure 3.1	Reaction scheme and proposed structure for complex Ni(gly)	31
Figure 3.2	Reaction scheme and proposed structure for complex Ni(ala)	32
Figure 3.3	Reaction scheme and proposed structure for complex Ni(his)	33
Figure 3.4	The appearance of the amino acid of nickel complexes	34
Figure 3.5	Coordination mode of the carboxylate ion to a metal ion	36
Figure 3.6	Infrared spectra of (a) glycine and (b) Ni(gly)	37
Figure 3.7	Infrared spectra of (a) alanine and (b) Ni(ala)	38
Figure 3.8	Infrared spectra of (a) L-Histidine and (b) Ni(his)	38
Figure 3.9	UV-Vis spectrum of Ni(gly), Ni(ala) and Ni(his)	41
Figure 3.10	Cyclic voltammogram of NiCl <sub>2</sub> .6H <sub>2</sub> O	43
Figure 3.11	Cyclic voltammogram of Ni(gly)	43
Figure 3.12	Cyclic voltammogram of Ni(ala)	44
Figure 3.13	Cyclic voltammogram of Ni(his)	44
Figure 3.14	TGA curves of Ni(gly)	45
Figure 3.15	The decomposition pathway diagram of Ni(gly)	47

Figure 3.16	TGA curves of Ni(ala)	48
Figure 3.17	The decomposition pathway diagram of Ni(ala)	49
Figure 3.18	TGA curves of Ni(his)	50
Figure 3.19	The decomposition pathway diagram of Ni(his)	52
Figure 3.20	The structure of diaquabis(glycine)nickel(II) dichloride [Ni(gly)], showing 50% probability displacement ellipsoids and the atomic numbering. Symmetry codes for the (A) $-x, -1/2 + y, -1/2 -z$ , (B) $-x, 1/2 + y, -1/2 -z$ and (C) $-x, -y, -z$ .	54
Figure 3.21	The crystal packing of diaquabis(glycine)nickel(II) dichloride [Ni(gly)], viewed along the $a$ axis showing the polymetric structure. Hydrogen bonds are drawn as dashed lines.	55
Figure 3.22	The crystal packing of diaquabis(glycine)nickel(II) dichloride [Ni(gly)], viewed along the $c$ axis showing the sheets running along the [010] direction. Hydrogen bonds are drawn as dashed line.	56
Figure 3.23	Crystal structure of diaquabis( $\beta$ -alanine-N,O)nickel(II) [Ni(ala)] (Jose <i>et al.</i> , 1964; Skoulka <i>et al.</i> , 1991)	59
Figure 3.24	Postulated structure of bis(L-histidinato)nickel(II) monohydrate [Ni(his)] (Sakurai <i>et al.</i> , 1978)	59
Figure 3.25	Electrophoresis results of incubating pBR322 with varying concentration of Ni(gly) with H <sub>2</sub> O <sub>2</sub> . Lane 1, DNA Ladder; lane 2, DNA alone; lane 3, DNA + H <sub>2</sub> O <sub>2</sub> ; lane 4, DNA+ 6.8 mM Ni(gly). Lane 5-12 involve DNA + H <sub>2</sub> O <sub>2</sub> + different concentration of Ni(gly): lane 5, 6.1 mM; 6, 6.2 mM; 7, 6.3 mM; 8, 6.4 mM; 9, 6.5 mM; 10, 6.6 mM, 11, 6.7 mM; and lane 12, 6.8 mM. Form I represents supercoiled DNA, Form II represents nicked DNA and Form III represents the linear DNA.	61
Figure 3.26	Electrophoresis results of incubating pBR322 with varying concentration of Ni(ala) with H <sub>2</sub> O <sub>2</sub> . Lane 1, DNA Ladder; lane 2, DNA alone; lane 3, DNA + H <sub>2</sub> O <sub>2</sub> ; lane 4, DNA + 7 mM Ni(ala). Lane 5-12 involve DNA + H <sub>2</sub> O <sub>2</sub> + different concentration of Ni(ala): lane 5, 6.3 mM; 6, 6.4 mM; 7, 6.5 mM; 8, 6.6 mM; 9, 6.7 mM; 10, 6.8 mM, 11, 6.9 mM; and lane 12, 7 mM.	62

Figure 3.27	Electrophoresis results of incubating pBR322 with varying concentration of Ni(his) with H <sub>2</sub> O <sub>2</sub> . Lane 1, DNA Ladder; lane 2, DNA alone; lane 3, DNA + H <sub>2</sub> O <sub>2</sub> ; lane 4, DNA + 5.2 mM Ni(his). Lane 5-12 involve DNA + H <sub>2</sub> O <sub>2</sub> + different concentration of Ni(his): lane 5, 4.5 mM; 6, 4.6 mM; 7, 4.7 mM; 8, 4.8 mM; 9, 4.9 mM; 10, 5 mM, 11, 5.1 mM; and lane 12, 5.2 mM.	62
Figure 3.28	Effect of radical scavengers on the reaction of DNA with 6.4 mM Ni(gly) and H <sub>2</sub> O <sub>2</sub> . Lane 1, DNA ladder; lane 2, DNA alone; lane 3, DNA + 6.4 mM Ni(gly); lane 4, DNA + 6.4 mM Ni(gly) + H <sub>2</sub> O <sub>2</sub> . Lane 5-10 involve reaction of Ni(gly) with DNA in presence of various scavengers; lane 5, 2 μL DMSO; lane 6, 1 mM D-mannitol; lane 7, 2 μL <i>tert</i> -butanol; lane 8, 1 mM KI; lane 9, 1 mM NaN <sub>3</sub> , and lane 10, 1.5 mM NaN <sub>3</sub> .	64
Figure 3.29	Effect of radical scavengers on the reaction of DNA with 6.5 mM Ni(ala) and H <sub>2</sub> O <sub>2</sub> . Lane 1, DNA ladder; lane 2, DNA alone; lane 3, DNA + 6.5 mM Ni(ala); lane 4, DNA + 6.5 mM Ni(ala) + H <sub>2</sub> O <sub>2</sub> . Lane 5-10 involve reaction of Ni(ala) with DNA in presence of various scavengers; lane 5, 2 μL DMSO; lane 6, 1 mM D-mannitol; lane 7, 2 μL <i>tert</i> -butanol; lane 8, 1 mM KI; lane 9, 1 mM NaN <sub>3</sub> , and lane 10, 1.5 mM NaN <sub>3</sub> .	64
Figure 3.30	Effect of radical scavengers on the reaction of DNA with 4.7 mM Ni(his) and H <sub>2</sub> O <sub>2</sub> . Lane 1, DNA ladder; lane 2, DNA alone; lane 3, DNA + 4.7 mM Ni(his); lane 4, DNA + 4.7 mM Ni(his) + H <sub>2</sub> O <sub>2</sub> . Lane 5-10 involve reaction of Ni(his) with DNA in presence of various scavengers; lane 5, 2 μL DMSO; lane 6, 1 mM D-mannitol; lane 7, 2 μL <i>tert</i> -butanol; lane 8, 1 mM KI; lane 9, 1 mM NaN <sub>3</sub> , and lane 10, 1.5 mM NaN <sub>3</sub> .	65
Figure 3.31	Reaction scheme and proposed structure for complex Ni(2- pic)	68
Figure 3.32	Reaction scheme and proposed structure for complex Ni(3,5-dinitro)	69
Figure 3.33	Reaction scheme and proposed structure for complex Ni(4-amino)	70
Figure 3.34	The appearance of the carboxylic acid of nickel complexes	71
Figure 3.35	Infrared spectra of (a) 2-picolinic acid and (b) Ni(2-pic)	73

		74
Figure 3.36	Infrared spectra of (a) 3,5-dinitrobenzoic acid and (b) Ni(3,5-dinitro)	74
Figure 3.37	Infrared spectra of (a) 4-aminobenzoic acid and (b) Ni(4-amino)	77
Figure 3.38	UV-Vis spectrum of Ni(2-pic), Ni(3,5-dinitro) and Ni(4-amino)	78
Figure 3.39	UV-Vis spectrum of Ni(2-pic), Ni(3,5-dinitro) and Ni(4-amino) for charge transfer transition	79
Figure 3.40	Cyclic voltammogram of Ni(2-pic)	80
Figure 3.41	Cyclic voltammogram of Ni(3,5-dinitro)	80
Figure 3.42	Cyclic voltammogram of Ni(4-amino)	81
Figure 3.43	TGA curves of Ni(2-Pic)	82
Figure 3.44	The decomposition pathway diagram of Ni(2-Pic)	83
Figure 3.45	TGA curves of Ni(3,5-dinitro)	85
Figure 3.46	The decomposition pathway diagram of Ni(3,5-dinitro)	86
Figure 3.47	TGA curves of Ni(4-amino)	87
Figure 3.48	The decomposition pathway diagram of Ni(4-amino)	88
Figure 3.49	Postulated structure of diaquabis(2-picolinato)nickel(II) dihydrate [Ni(2-pic)] (Loiseleur ,1972)	89
Figure 3.50	Crystal structure of tetraaquabis(3,5-dinitrobenzoato)nickel(II) tetrahydrate [Ni(3,5-dinitro)] (Chen <i>et al.</i> , 2006)	89
Figure 3.51	Postulated structure of diaquabis(4-aminobenzoato)nickel(II) [Ni(4-amino)] (Amiraslanov <i>et al.</i> , 1978)	91
Figure 3.52	Electrophoresis results of incubating pBR322 with varying concentration of Ni(2-pic) with H <sub>2</sub> O <sub>2</sub> . Lane 1, DNA Ladder; lane 2, DNA alone; lane 3, DNA + H <sub>2</sub> O <sub>2</sub> ; lane 4, DNA + 5.5 mM Ni(2-pic). Lane 5-12 involve DNA + H <sub>2</sub> O <sub>2</sub> + different concentration of Ni(2-pic): lane 5, 4.8 mM; 6, 4.9 mM; 7, 5.0 mM; 8, 5.1 mM; 9, 5.2 mM; 10, 5.3 mM, 11, 5.4 mM; and lane 12, 5.5 mM.	



- Figure 3.53 Electrophoresis results of incubating pBR322 with varying concentration of Ni(3,5-dinitro) with H<sub>2</sub>O<sub>2</sub>. Lane 1, DNA Ladder; lane 2, DNA alone; lane 3, DNA + H<sub>2</sub>O<sub>2</sub>; lane 4, DNA + 10 mM Ni(3,5-dinitro). Lane 5-12 involve DNA + H<sub>2</sub>O<sub>2</sub> + different concentration of Ni(3,5-dinitro): lane 5, 0.006 mM; 6, 0.01 mM; 7, 0.06 mM; 8, 0.1 mM; 9, 0.6 mM; 10, 1.0 mM, 11, 6.0 mM; and lane 12, 10 mM. 92
- Figure 3.54 Electrophoresis results of incubating pBR322 with varying concentration of Ni(4-amino) with H<sub>2</sub>O<sub>2</sub>. Lane 1, DNA Ladder; lane 2, DNA alone; lane 3, DNA + H<sub>2</sub>O<sub>2</sub>; lane 4, DNA + 3.9 mM Ni(4-amino). Lane 5-12 involve DNA + H<sub>2</sub>O<sub>2</sub> + different concentration of Ni(4-amino): lane 5, 3.2 mM; 6, 3.3 mM; 7, 3.4 mM; 8, 3.5 mM; 9, 3.6 mM; 10, 3.7 mM, 11, 3.8 mM; and lane 12, 3.9 mM. 93
- Figure 3.55 Effect of radical scavengers on the reaction of DNA with 5.1 mM Ni(2-pic) and H<sub>2</sub>O<sub>2</sub>. Lane 1, DNA ladder; lane 2, DNA alone; lane 3, DNA + 5.1 mM Ni(2-pic); lane 4, DNA + 5.1 mM Ni(2-pic) + H<sub>2</sub>O<sub>2</sub>. Lane 5-10 involve reaction of Ni(2-pic) with DNA in presence of various scavengers; lane 5, 2 μL DMSO; lane 6, 1 mM D-mannitol; lane 7, 2 μL *tert*-butanol; lane 8, 1 mM KI; lane 9, 1 mM NaN<sub>3</sub>, and lane 10, 1.5 mM NaN<sub>3</sub>. 93
- Figure 3.56 Effect of radical scavengers on the reaction of DNA with 0.1 mM Ni(3,5-dinitro) and H<sub>2</sub>O<sub>2</sub>. Lane 1, DNA ladder; lane 2, DNA alone; lane 3, DNA + 0.1 mM Ni(3,5-dinitro); lane 4, DNA + 0.1 mM Ni(3,5-dinitro) + H<sub>2</sub>O<sub>2</sub>. Lane 5-10 involve reaction of Ni(3,5-dinitro) with DNA in presence of various scavengers; lane 5, 2 μL DMSO; lane 6, 1 mM D-mannitol; lane 7, 2 μL *tert*-butanol; lane 8, 1 mM KI; lane 9, 1 mM NaN<sub>3</sub>, and lane 10, 1.5 mM NaN<sub>3</sub>. 94
- Figure 3.57 Effect of radical scavengers on the reaction of DNA with 3.3 mM Ni(4-amino) and H<sub>2</sub>O<sub>2</sub>. Lane 1, DNA ladder; lane 2, DNA alone; lane 3, DNA + 3.3 mM Ni(4-amino); lane 4, DNA + 3.3 mM Ni(4-amino) + H<sub>2</sub>O<sub>2</sub>. Lane 5-10 involve reaction of Ni(4-amino) with DNA in presence of various scavengers; lane 5, 2 μL DMSO; lane 6, 1 mM D-mannitol; lane 7, 2 μL *tert*-butanol; lane 8, 1 mM KI; lane 9, 1 mM NaN<sub>3</sub>, and lane 10, 1.5 mM NaN<sub>3</sub>. 96
- Figure 3.58 Reaction scheme and proposed structure for complex Ni(pyr) 97
- Figure 3.59 Reaction scheme and proposed structure for complex

	Fe(pyr)	98
Figure 3.60	The appearance of the Ni(pyr) and Fe(pyr) complexes	100
Figure 3.61	Infrared spectra of (a) pyrazine-2-carboxylic acid and (b) Ni(pyr)	100
Figure 3.62	Infrared spectra of (a) pyrazine-2-carboxylic acid and (b) Fe(pyr)	103
Figure 3.63	UV-Vis spectrum of Ni(pyr)	103
Figure 3.64	UV-Vis spectrum of Fe(pyr)	105
Figure 3.65	Cyclic voltammogram of Ni(pyr)	105
Figure 3.66	Cyclic voltammogram of FeCl <sub>2</sub> .4H <sub>2</sub> O	106
Figure 3.67	Cyclic voltammogram of Fe(pyr)	107
Figure 3.68	TGA curves of Ni(pyr)	108
Figure 3.69	The decomposition pathway diagram of Ni(pyr)	109
Figure 3.70	TGA curves of Fe(pyr)	110
Figure 3.71	The decomposition pathway diagram of Fe(pyr)	111
Figure 3.72	Crystal structure of diaquabis(2-pyrazinecarboxylato) nickel(II) [Ni(pyr)] (Ptasiewicz-Bak <i>et al.</i> , 1995; El-Medani <i>et al.</i> , 2005)	111
Figure 3.73	Postulated structure of diaquabis(2-pyrazinecarboxylato) iron(II) pyrazine hemisolvate [Fe(pyr)]	113
Figure 3.74	Electrophoresis results of incubating pBR322 with varying concentration of Ni(pyr) with H <sub>2</sub> O <sub>2</sub> . Lane 1, DNA Ladder; lane 2, DNA alone; lane 3, DNA + H <sub>2</sub> O <sub>2</sub> ; lane 4, DNA + 8 mM Ni(pyr). Lane 5-12 involve DNA + H <sub>2</sub> O <sub>2</sub> + different concentration of Ni(pyr): lane 5, 1 mM; 6, 2 mM; 7, 3 mM; 8, 4 mM; 9, 5 mM; 10, 6 mM, 11, 7 mM; and lane 12, 8 mM.	113
Figure 3.75	Electrophoresis results of incubating pBR322 with varying concentration of Fe(pyr) with H <sub>2</sub> O <sub>2</sub> . Lane 1, DNA Ladder; lane 2, DNA alone; lane 3, DNA + H <sub>2</sub> O <sub>2</sub> ; lane 4, DNA + 3 mM Fe(pyr). Lane 5-12 involve DNA + H <sub>2</sub> O <sub>2</sub> + different concentration of Fe(pyr): lane 5, 2.3 mM; 6, 2.4 mM; 7, 2.5 mM; 8, 2.6 mM; 9, 2.7 mM; 10, 2.8 mM, 11, 2.9 mM; and lane 12, 3 mM.	

		114
Figure 3.76	Effect of radical scavengers on the reaction of DNA with 5 mM Ni(pyr) and H <sub>2</sub> O <sub>2</sub> . Lane 1, DNA ladder; lane 2, DNA alone; lane 3, DNA + 5 mM Ni(pyr); lane 4, DNA + 5 mM Ni(pyr) + H <sub>2</sub> O <sub>2</sub> . Lane 5-10 involve reaction of Ni(pyr) with DNA in presence of various scavengers; lane 5, 2 μL DMSO; lane 6, 1 mM D-mannitol; lane 7, 2 μL <i>tert</i> -butanol; lane 8, 1 mM KI; lane 9, 1 mM NaN <sub>3</sub> , and lane 10, 1.5 mM NaN <sub>3</sub> .	115
Figure 3.77	Effect of radical scavengers on the reaction of DNA with 2.8 mM Fe(pyr) and H <sub>2</sub> O <sub>2</sub> . Lane 1, DNA ladder; lane 2, DNA alone; lane 3, DNA + 2.8 mM Fe(pyr); lane 4, DNA + 2.8 mM Fe(pyr) + H <sub>2</sub> O <sub>2</sub> . Lane 5-10 involve reaction of Fe(pyr) with DNA in presence of various scavengers; lane 5, 2 μL DMSO; lane 6, 1 mM D-mannitol; lane 7, 2 μL <i>tert</i> -butanol; lane 8, 1 mM KI; lane 9, 1 mM NaN <sub>3</sub> , and lane 10, 1.5 mM NaN <sub>3</sub> .	117
Figure 3.78	Reaction scheme and proposed structure for complex Ni(mal)	118
Figure 3.79	Reaction scheme and proposed structure for complex Fe(mal)	119
Figure 3.80	The appearance of the Ni(mal) and Fe(mal) complexes	121
Figure 3.81	Infrared spectra of (a) maleic acid and (b) Ni(mal)	121
Figure 3.82	Infrared spectra of (a) maleic acid and (b) Fe(mal)	124
Figure 3.83	UV-Vis spectrum of Ni(mal)	124
Figure 3.84	UV-Vis spectrum of Fe(mal)	126
Figure 3.85	Cyclic voltammogram of Ni(mal)	126
Figure 3.86	Cyclic voltammogram of Fe(mal)	127
Figure 3.87	TGA curves of Ni(mal)	128
Figure 3.88	The decomposition pathway diagram of Ni(mal)	129
Figure 3.89	TGA curves of Fe(mal)	131
Figure 3.90	The decomposition pathway diagram of Fe(mal)	132
Figure 3.91	Crystal structure of tetraaquabis(maleato)nickel(II) [Ni(mal)] (Gupta <i>et al.</i> , 1984; Zhou <i>et al.</i> , 1987;	

	Sequeira <i>et al.</i> , 1992)	132
Figure 3.92	Postulated structure of tetraaquabis(maleato)iron(II) [Fe(mal)] (Gupta <i>et al.</i> , 1977; Porollo <i>et al.</i> , 1997; Barman <i>et al.</i> , 2002)	134
Figure 3.93	Electrophoresis results of incubating pBR322 with varying concentration of Ni(mal) with H <sub>2</sub> O <sub>2</sub> . Lane 1, DNA Ladder; lane 2, DNA alone; lane 3, DNA + H <sub>2</sub> O <sub>2</sub> ; lane 4, DNA + 10 mM Ni(mal). Lane 5-12 involve DNA + H <sub>2</sub> O <sub>2</sub> + different concentration of Ni(mal): lane 5, 3 mM; 6, 4 mM; 7, 5 mM; 8, 6 mM; 9, 7 mM; 10, 8 mM, 11, 9 mM; and lane 12, 10 mM.	134
Figure 3.94	Electrophoresis results of incubating pBR322 with varying concentration of Fe(mal) with H <sub>2</sub> O <sub>2</sub> . Lane 1, DNA Ladder; lane 2, DNA alone; lane 3, DNA + H <sub>2</sub> O <sub>2</sub> ; lane 4, DNA + 4.1 mM Fe(mal). Lane 5-12 involve DNA + H <sub>2</sub> O <sub>2</sub> + different concentration of Fe(mal): lane 5, 3.4 mM; 6, 3.5 mM; 7, 3.6 mM; 8, 3.7 mM; 9, 3.8 mM; 10, 3.9 mM, 11, 4.0 mM; and lane 12, 4.1 mM.	135
Figure 3.95	Effect of radical scavengers on the reaction of DNA with 6 mM Ni(mal) and H <sub>2</sub> O <sub>2</sub> . Lane 1, DNA ladder; lane 2, DNA alone; lane 3, DNA + 6 mM Ni(mal); lane 4, DNA + 6 mM Ni(mal) + H <sub>2</sub> O <sub>2</sub> . Lane 5-10 involve reaction of Ni(mal) with DNA in presence of various scavengers; lane 5, 2 $\mu$ L DMSO; lane 6, 1 mM D-mannitol; lane 7, 2 $\mu$ L <i>tert</i> -butanol; lane 8, 1 mM KI; lane 9, 1 mM NaN <sub>3</sub> , and lane 10, 1.5 mM NaN <sub>3</sub> .	136
Figure 3.96	Effect of radical scavengers on the reaction of DNA with 3.5 mM Fe(mal) and H <sub>2</sub> O <sub>2</sub> . Lane 1, DNA ladder; lane 2, DNA alone; lane 3, DNA + 3.5 mM Fe(mal); lane 4, DNA + 3.5 mM Fe(mal) + H <sub>2</sub> O <sub>2</sub> . Lane 5-10 involve reaction of Fe(mal) with DNA in presence of various scavengers; lane 5, 2 $\mu$ L DMSO; lane 6, 1 mM D-mannitol; lane 7, 2 $\mu$ L <i>tert</i> -butanol; lane 8, 1 mM KI; lane 9, 1 mM NaN <sub>3</sub> , and lane 10, 1.5 mM NaN <sub>3</sub> .	139
Figure 3.97	Reaction scheme and proposed structure for complex Ni(pdc)	140
Figure 3.98	Reaction scheme and proposed structure for complex Fe(pdc)	141
Figure 3.99	The appearance of the Ni(pdc) and Fe(pdc) complexes	143
Figure 3.100	Infrared spectra of (a) pyridine-2,6-dicarboxylic acid and (b) Ni(pdc)	

		143
Figure 3.101	Infrared spectra of (a) pyridine-2,6-dicarboxylic acid and (b) Fe(pdc)	146
Figure 3.102	UV-Vis spectrum of Ni(pdc)	146
Figure 3.103	UV-Vis spectrum of Fe(pdc)	148
Figure 3.104	Cyclic voltammogram of Ni(pdc)	148
Figure 3.105	Cyclic voltammogram of FeCl <sub>3</sub>	149
Figure 3.106	Cyclic voltammogram of Fe(pdc)	150
Figure 3.107	TGA curves of Ni(pdc)	151
Figure 3.108	The propose decomposition pathway diagram of Ni(pdc)	152
Figure 3.109	TGA curves of Fe(pdc)	153
Figure 3.110	The decomposition pathway diagram of Fe(pdc)	154
Figure 3.111	Crystal structure of dipotassium bis(pyridine-2,6-dicarboxylato)nickel(II) heptahydrate [Ni(pdc)] (Nathan and Mai, 2000)	154
Figure 3.112	Crystal structure of hydronium bis(pyridine-2,6-dicarboxylato)iron(III) [Fe(pdc)] (Cousson <i>et al.</i> , 1992; Marsh, 1993)	156
Figure 3.113	Electrophoresis results of incubating pBR322 with varying concentration of Ni(pdc) with H <sub>2</sub> O <sub>2</sub> . Lane 1, DNA Ladder; lane 2, DNA alone; lane 3, DNA + H <sub>2</sub> O <sub>2</sub> ; lane 4, DNA + 8 mM Ni(pdc). Lane 5-12 involve DNA + H <sub>2</sub> O <sub>2</sub> + different concentration of Ni(pdc): lane 5, 1 mM; 6, 2 mM; 7, 3 mM; 8, 4 mM; 9, 5 mM; 10, 6 mM, 11, 7 mM; and lane 12, 8 mM.	156
Figure 3.114	Electrophoresis results of incubating pBR322 with varying concentration of Fe(pdc) with H <sub>2</sub> O <sub>2</sub> . Lane 1, DNA Ladder; lane 2, DNA alone; lane 3, DNA + H <sub>2</sub> O <sub>2</sub> ; lane 4, DNA + 1.3 mM Fe(pdc). Lane 5-12 involve DNA + H <sub>2</sub> O <sub>2</sub> + different concentration of Fe(pdc): lane 5, 0.6 mM; 6, 0.7 mM; 7, 0.8 mM; 8, 0.9 mM; 9, 1.0 mM; 10, 1.1 mM, 11, 1.2 mM; and lane 12, 1.3 mM.	

Figure 3.115 Effect of radical scavengers on the reaction of DNA with 2 mM Ni(pdc) and H<sub>2</sub>O<sub>2</sub>. Lane 1, DNA ladder; lane 2, DNA alone; lane 3, DNA + 2 mM Ni(pdc); lane 4, DNA + 2 mM Ni(pdc) + H<sub>2</sub>O<sub>2</sub>. Lane 5-10 involve reaction of Ni(pdc) with DNA in presence of various scavengers; lane 5, 2 μL DMSO; lane 6, 1 mM D-mannitol; lane 7, 2 μL *tert*-butanol; lane 8, 1 mM KI; lane 9, 1 mM NaN<sub>3</sub>, and lane 10, 1.5 mM NaN<sub>3</sub>.

158

Figure 3.116 Effect of radical scavengers on the reaction of DNA with 1.1 mM Fe(pdc) and H<sub>2</sub>O<sub>2</sub>. Lane 1, DNA ladder; lane 2, DNA alone; lane 3, DNA + 1.1 mM Fe(pdc); lane 4, DNA + 1.1 mM Fe(pdc) + H<sub>2</sub>O<sub>2</sub>. Lane 5-10 involve reaction of Fe(pdc) with DNA in presence of various scavengers; lane 5, 2 μL DMSO; lane 6, 1 mM D-mannitol; lane 7, 2 μL *tert*-butanol; lane 8, 1 mM KI; lane 9, 1 mM NaN<sub>3</sub>, and lane 10, 1.5 mM NaN<sub>3</sub>.

## LIST OF ABBREVIATIONS

DNA	Deoxyribonucleic Acid
ROS	Reactive Oxygen Species
IARC	International Agency for Research on Cancer
FT-IR	Fourier Transform Infrared Spectroscopy
CHN	Carbon, Hydrogen, Nitrogen
AAS	Atomic Absorption Spectroscopy
UV-Vis	Ultraviolet-Visible Spectrometry
CV	Cyclic Voltammetry
TGA	Thermogravimetric Analysis
IC <sub>50</sub>	Fifty percent cytotoxic dose
S.E.M	Standard error of the mean
MTT	3-(4, 5-dimethylthiazol-2-yl)-2, 5-diphenyltetrazolium bromide
LMCT	Ligand to metal charge transfer
DMSO	Dimethyl sulfoxide
Gly	Glycine
Ala	$\beta$ -alanine
His	L-histidine
Ni(gly)	Diaquabis(glycine)nickel(II) dichloride
Ni(ala)	Diaquabis( $\beta$ -alanine-N,O)nickel(II)
Ni(his)	Bis(L-histidinato)nickel(II) monohydrate
2-pic	2-picolinic acid
3,5-dinitro	3,5-dinitrobenzoic acid

4-amino	4-aminobenzoic acid
Ni(2-pic)	Diaquabis(2-picolinato)nickel(II) dihydrate
Ni(3,5-dinitro)	Tetraaquabis(3,5-dinitrobenzoato)nickel(II) tetrahydrate
Ni(4-amino)	Diaquabis(4-aminobenzoato)nickel(II)
Pyr	Pyrazine-2-carboxylic acid
Ni(pyr)	Diaquabis(2-pyrazinecarboxylato)nickel(II)
Fe(pyr)	Diaquabis(2-pyrazinecarboxylato)iron(II) pyrazine hemisolvate
Mal	Maleic acid
Ni(mal)	Tetraaquabis(maleato)nickel(II)
Fe(mal)	Tetraaquabis(maleato)iron(II)
Pdc	Pyridine-2,6-dicarboxylic acid
Ni(pdc)	Dipotassium bis(pyridine-2,6-dicarboxylato)nickel(II) heptahydrate
Fe(pdc)	Hydronium bis(pyridine-2,6-dicarboxylato)iron(III)



# **SINTESIS, PENCIRIAN DAN SIFAT BIOLOGI KOMPLEKS NIKEL- DAN FERUM- KARBOKSILAT**

## **ABSTRAK**

Dalam projek penyelidikan ini, sembilan kompleks Ni(II) telah berjaya disintesis daripada tindak balas antara nikel(II) klorida heksahidrat,  $\text{NiCl}_2 \cdot 6\text{H}_2\text{O}$  dengan ligan asid amino (glisina,  $\beta$ -alanina dan L-histidina), ligan asid karboksilik (asid 2-pikolinik, asid 3,5-dinitrobenzoik, asid 4-aminobenzoik dan asid pirazina-2-karboksilik) dan ligan asid dikarboksilik (asid maleik dan asid piridina-2,6-dikarboksilik). Selain itu, dua kompleks Fe(II) dan satu kompleks Fe(III) juga telah berjaya disintesis. Kompleks Fe(II) disintesis daripada tindak balas antara ferum(II) klorida 4-hidrat,  $\text{FeCl}_2 \cdot 4\text{H}_2\text{O}$  dengan ligan asid pirazina-2-karboksilik dan asid maleik masing-masing. Manakala kompleks Fe(III) disintesis daripada tindak balas ferum(III) klorida dengan ligan asid piridina-2,6-dikarboksilik. Nisbah stoikiometri logam kepada ligan yang digunakan ialah 1:2. Kompleks-kompleks ini dicirikan melalui analisis takat lebur, keterlarutan, konduktiviti, Spektroskopi Inframerah (IR), Mikroanalisis CHN, Spektroskopi Penyerapan Atom (AAS), Spektroskopi Ultralembayung Ungu (UV-Vis), Analisis Siklik Voltammetrik (CV), Analisis Termogravimetrik (TGA) dan X-ray Kristalografi. Selain itu, interaksi antara kompleks logam dengan DNA pBR322 juga dikaji melalui eksperimen gel elektroforesis, manakala aktiviti sitotoksik kompleks logam tersebut pula dikaji melalui pengasaian MTT. Analisis keputusan IR menunjukkan kesemua ligan terikat secara monodentat kepada atom pusat Ni dan Fe melalui kumpulan  $\text{COO}^-$ . Analisis

UV-Vis menunjukkan bahawa keadaan pengoksidaan bagi nikel dalam kompleks ialah +2 dan mempunyai konfigurasi  $d^8$  manakala kompleks Fe(II) dan Fe(III) mempunyai keadaan pengoksidaan +2 dan +3 dan konfigurasi  $d^6$  dan  $d^5$  masing-masing. Analisis CV menunjukkan bahawa semua kompleks mempunyai sifat redoks pembalikan yang penting dalam kegunaan biologi. Hasil kajian eksperimen gel elektroforesis menunjukkan kesemua kompleks logam berjaya membuat pemotongan plasmid DNA dimana pemotongan tersebut menghasilkan jalur tunggal serta jalur berganda DNA sebagai produk. Keberkesanan pemotongan plasmid DNA ini bergantung kepada kepekatan kompleks logam tersebut. Kompleks ferum mempamerkan keberkesanan pemotongan yang lebih efisien berbanding dengan kompleks nikel (II). Dalam keputusan pengasaian MTT, kesemua kompleks logam menunjukkan aktiviti sitotoksik terhadap sel turunan kanser HepG2.

**SYNTHESIS, CHARACTERIZATION AND BIOLOGICAL PROPERTIES  
OF NICKEL- AND IRON- CARBOXYLATE COMPLEXES**

**ABSTRACT**

In this research, nine Ni(II) complexes were successfully synthesized using nickel(II) chloride hexahydrate,  $\text{NiCl}_2 \cdot 6\text{H}_2\text{O}$  with amino acids (Glycine,  $\beta$ -alanine and L-histidine), carboxylic acids (2-picolinic acid, 3,5-dinitrobenzoic acid, 4-aminobenzoic acid and pyrazine-2-carboxylic acid) and with dicarboxylic acids (maleic acid and pyridine-2,6-dicarboxylic acid). Besides, two Fe(II) complexes and one Fe(III) complexes were also successfully synthesized. Fe(II) complexes were synthesized using iron(II) chloride 4-hydrate,  $\text{FeCl}_2 \cdot 4\text{H}_2\text{O}$  with pyrazine-2-carboxylic acid and maleic acid respectively. While Fe(III) complex was synthesized using ferric chloride anhydrous,  $\text{FeCl}_3$  with pyridine-2,6-dicarboxylic acid. Stoichiometry ratio of metal to ligand being used is 1:2. These complexes were characterized by determination of melting point, solubility, conductivity measurement, Fourier Transform Infrared Spectroscopy (FTIR), CHN microanalysis, Analysis of Atomic Absorption Spectroscopy (AAS), Ultraviolet-Visible Spectrometry (UV-Vis), Cyclic Voltammetry (CV), Thermogravimetric Analysis (TGA) and X-ray crystallography. Besides that, the interaction between the metal complexes and pBR322 DNA will be investigated by gel electrophoresis experiments, while the cytotoxic activity of the complexes was tested by MTT Assay. FT-IR analysis result shows that the carboxylate group in all of the ligand were coordinated to the central metal ion monodentately. The UV-Vis analysis shows that the oxidation state for nickel complexes is +2 and its configuration system is  $d^8$

meanwhile the oxidation state for Fe(II) and Fe(III) complexes are +2 and +3 and configuration systems are  $d^6$  and  $d^5$  respectively. The CV analysis shows that all the complexes have reversible redox properties which are very important in biological uses. Gel electrophoresis experiments show that all the complexes successfully promote the cleavage of plasmid DNA, producing single and double DNA strand breaks. In MTT assay results, all of the complexes showed cytotoxic activity against HepG2 cancer cell lines.

# CHAPTER 1

## INTRODUCTION

### 1.1 Nickel

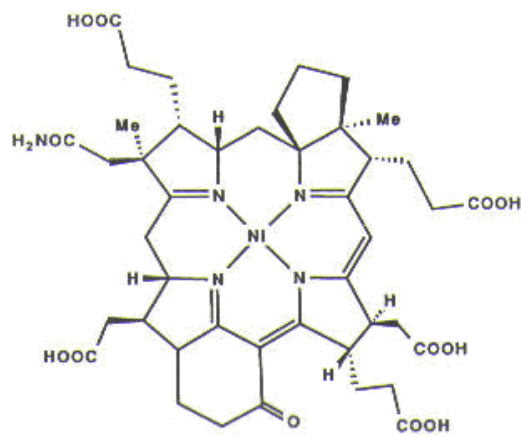
Nickel is a transition metal with the symbol Ni and atomic number 28. It is a silvery white metal that takes on a high polish. It is hard, malleable, ductile, ferromagnetic, and a fair conductor of heat and electricity. Nickel can form a number of complex compounds. Many of these nickel compounds are water soluble and have a characteristic green or blue color. Nickel and its compounds have no characteristic odor or taste. The most common oxidation state of nickel is +2, though 0, +1, +3 and +4 Ni complexes are observed.

#### 1.1.1 Applications of Nickel

Properties of nickel make it very desirable for combining with other metals to form mixtures called alloys. Some of the metals that nickel can be alloyed with are iron, copper, chromium, and zinc. These alloys are used in making metal coins and jewellery and in industry for making items such as valves and heat exchangers. Nickel is mostly used to make stainless steel. There are also compounds consisting of nickel combined with many other elements, including chlorine, sulfur, and oxygen. Nickel compounds are used for nickel plating, to color ceramics, to make some batteries, and as catalysts to increase the rate of chemical reactions.

Besides, nickel is required for the function of several enzymes in the human body. Nickel is found in factor F430, which is required for methanogenesis, a process used by the archaeobacteria in which the simple gases, such as H<sub>2</sub>, CO, and

CO<sub>2</sub>, are used to provide both energy and a carbon source (Figure 1.1) (Crabtree, 1988; Lippard and Berg, 1994).



Factor F<sub>430</sub>

Figure 1.1 Metals in biological systems: nickel in factor F<sub>430</sub>

## 1.2 Iron

Iron is a chemical element with the symbol Fe and atomic number 26. Iron is a lustrous, ductile, malleable and silver-grey metal. It is one of the few ferromagnetic elements. It is known to exist in four distinct crystalline forms. Iron rusts in damp air, but not in dry air. It dissolves readily in dilute acids. Iron is chemically active and forms two major series of chemical compounds, the bivalent iron (II), or ferrous, compounds and the trivalent iron (III), or ferric, compounds.

### 1.2.1 Applications of Iron

Iron is the most widely used of all the metals, accounting for 95% of worldwide metal production. Its low cost and high strength make it indispensable in engineering applications such as the construction of machinery and machine tools, automobiles, the hulls of large ships, and structural components for buildings. Since pure iron is quite soft, it is most commonly used in the form of steel. Some of

the forms in which iron is produced commercially include cast iron, wrought iron, carbon steel, alloy steels, iron(III) oxides.

In biological system, iron is found in a variety of iron-sulfur clusters, which are necessary for nitrogen fixation, as well as in heme groups, found in hemoglobin, which is used for dioxygen transport and storage in the body (Figure 1.2) (Crabtree, 1988; Lippard and Berg, 1994).

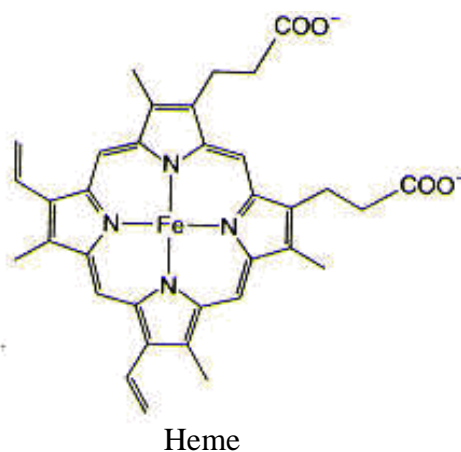


Figure 1.2 Metals in biological systems: iron in heme, which is found in hemoglobin

### 1.3 Transition Metal Complexes

Transition metal complexes have been the subject of thorough investigation because of their extensive applications in wide ranging areas from material sciences to biological sciences (Boerner and Zaleski, 2005). Metal complexes are well-known to accelerate the drug action and the efficacy of a therapeutic agent can often be enhanced upon coordination with a metal ion (Goldstein *et al.*, 1986). The pharmacological activity has also been found to be highly dependent on the nature of the metal ion and the donor sequence of the ligands as different ligands exhibit different biological properties (Delaney *et al.*, 2002). In recent years, the binding studies of transition metal complexes have become an important field in the

development of DNA molecular probes and chemotherapeutics (Dardlier *et al.*, 1997).

The carboxylate group is an important class of ligand in inorganic and bioinorganic chemistry. Metal complexes containing monocarboxylic acids are well known and the publication of many structurally characterised examples of this class of compound has demonstrated the versatility of the carboxylate group as an innersphere ligand (Mehrotra and Bohra, 1983).

The chemistry of nickel (II) complexes with simple carboxylate anions has been widely studied (Sacconi *et al.*, 1987; Oldham, 1968). And several examples of dicarboxylate complexes of this metal have also been described (Krisnamurty and Harris, 1961). The versatility in coordination modes exhibited by these kinds of ligands, together with their ability to form polymeric species make its structural chemistry particularly interesting. Related systems with another function besides the carboxylate group like pyridine-2 carboxylate, glycine and 2-aminobenzoic acid have also received recent attention (D'Avignon and Brown, 1982; Carmona *et al.*, 1990; Zhong *et al.*, 1994; Abbot *et al.*, 1995).

#### **1.4 DNA**

DNA, or deoxyribonucleic acid, is the hereditary material in humans and almost all other organisms. Nearly every cell in a person's body has the same DNA. Most DNA is located in the cell nucleus (where it is called nuclear DNA), but a small amount of DNA can also be found in the mitochondria (where it is called mitochondrial DNA or mtDNA).

The information in DNA is stored as a code made up of four chemical bases: adenine(A), guanine(G), cytosine(C), and thymine(T). Human DNA consists of



about 3 billion bases, and more than 99 percent of those bases are the same in all people. The order, or sequence, of these bases determines the information available for building and maintaining an organism, similar to the way in which letters of the alphabet appear in a certain order to form words and sentences.

DNA bases pair up with each other, A with T and C with G, to form units called base pairs. Each base is also attached to a sugar molecule and a phosphate molecule. Together, a base, sugar, and phosphate are called a nucleotide. Nucleotides are arranged in two long strands that form a spiral called a double helix (Figure 1.3). The structure of the double helix is somewhat like a ladder, with the base pairs forming the ladder's rungs and the sugar and phosphate molecules forming the vertical side pieces of the ladder.

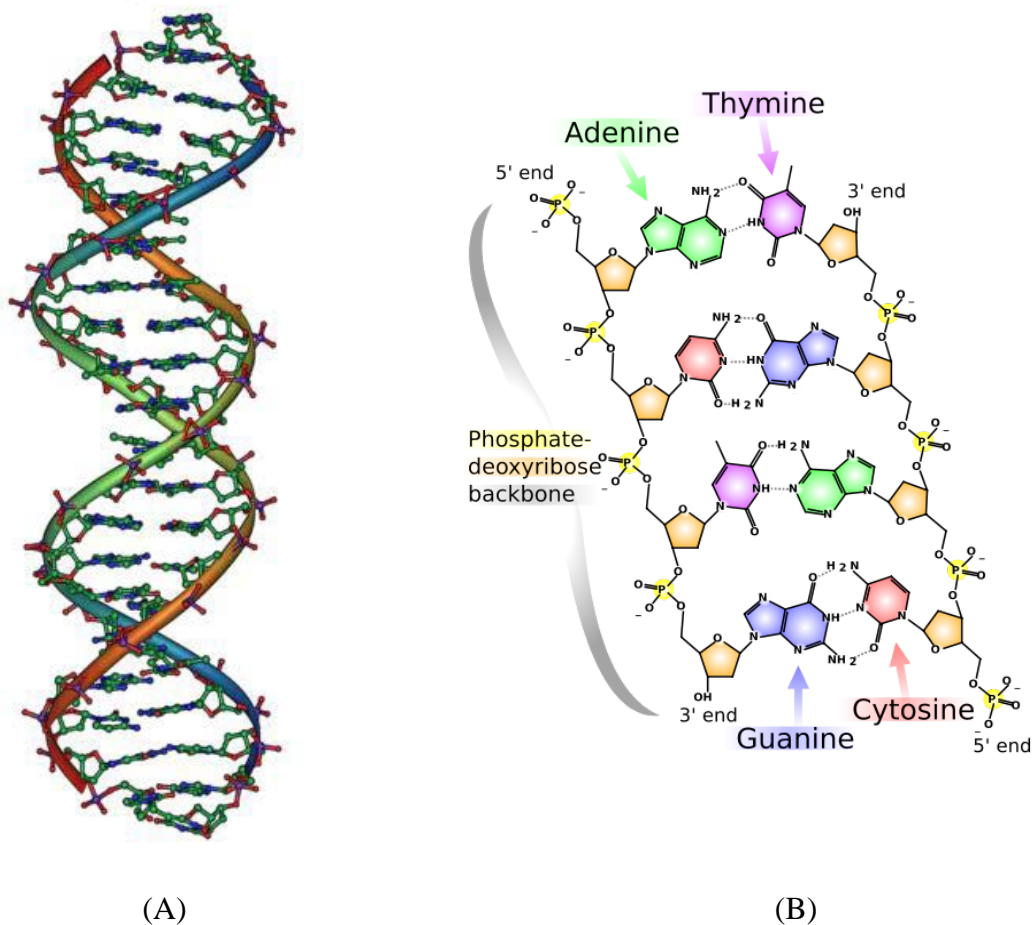


Figure 1.3 (A) The structure of part of a DNA double helix (B) The chemical structure of DNA (<http://schools-wikipedia.org/wp/d/DNA.htm>)

## 1.5 The Interaction of Transition Metal Complexes and DNA

Transition metal complexes have been of interest in the field of cancer research. They had been widely studied for their antimicrobial and anticancer properties. This is because they exhibit unique spectral and electrochemical signatures, as well as the ability of their ligands to be modulated to DNA binding and cleaving abilities.

Many biological studies suggest that DNA is the primary intracellular target of anticancer drugs because of the interactions between small molecules and DNA can often cause DNA damage in cancer cells, blocking the division of cancer cells and resulting in cell death (Hecht, 2000). Of those studies, the interaction of transition metal complexes with DNA has gained much attention owing to their possible application as new therapeutic agents (Metcalf and Thomas, 2003).

A number of transition metal complexes with planar aromatic heterocyclic ligands have been used as probes of DNA secondary structure and therapeutic agents, and the biological activities of these DNA targeted complexes usually increase compared with those of either free ligands or metal ions alone, which may be due to different binding properties of these complexes to DNA (Lewandowski *et al.*, 2005). The type of central metal ions, which is responsible for the geometry of complexes, also has significant influence on the intercalating ability of transition metal complexes to DNA (Chaires, 1997; Mozaffar *et al.*, 2004).

It is believed that the biological activity of antitumor metal complexes is strictly connected to their abilities to bind to DNA, damage DNA structures and impair DNA functions (Burrows and Rokita, 1994). Impairment of DNA function results in inhibition of replication and transcription process and even in cell death, if

eventually the DNA lesions are not rapidly and properly repaired (Sitlani *et al.*, 1992; Li *et al.*, 2005).

Basically, transition metal complexes interact with double helix DNA in either noncovalent or covalent way. Concerning the noncovalent interactions between transition metal complexes and DNA, they can occur by intercalation, groove binding, or external electrostatic binding. Intercalation consists of the insertion of a flat aromatic molecule between two adjacent bases. Groove binding is a stronger type of interaction that takes place when a molecule of proper size enters one of the grooves of DNA. External electrostatic binding refers to those interactions that occur on the DNA surface, mainly governed by electrostatic effects. Among these interactions, intercalation is one of the most important DNA binding modes. It was reported that the intercalating ability appeared to increase with the planarity of ligands.

Specifically we investigated the interaction between the metal complex and DNA by gel electrophoresis. When circular plasmid DNA is conducted by electrophoresis, the fastest migration will be observed for the supercoiled form (Form I). If one strand is cleaved, the supercoiled form will relax to produce a slower moving nicked circular form (Form II) (An *et al.*, 2006). If both strands are cleaved, a linear form (Form III) will be generated that migrates in between (Masataka *et al.*, 1999). Hence, DNA strand breaks were quantified by measuring the transformation of the supercoiled form into nicked circular and linear forms (Figure 1.4).

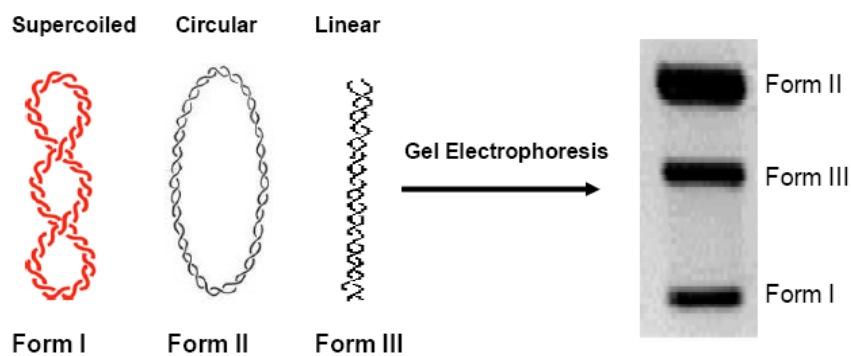


Figure 1.4 Three forms of DNA that can be tracked using agarous gel electrophoresis

## 1.6 Transition Metal Complexes as Anticancer Agents

In the history of coordination complexes in cancer therapy, the first transition metal to be used successfully as an anticancer agent was platinum. It was used in a compound  $\text{cis-}[\text{Pt}(\text{NH}_3)_2\text{Cl}_2]$  or cisplatin (Figure 1.5). Its ability to inhibit tumors was discovered by Rosenberg around 1969 (Rosenberg *et al.*, 1969 & 1970). Cisplatin entered clinical trials in 1971 and was approved by the FDA in 1978 (Higby *et al.*, 1974). It has become one of the most widely used drugs in cancer chemotherapy. The platinum drugs such as carboplatin, nedaplatin and oxaliplatin (Figure 1.6) are frequently used in combination therapy for numerous solid tumours, including ovarian, head and neck, testicular, bladder, colorectal, gastric, melanoma and small-cell lung cancer (Giaccone, 2000).

Systemic toxicity of cisplatin gives rise to a number of limitations. Serious side-effects such as nausea, nephrotoxicity, neurotoxicity and ototoxicity occur often (Reedijk, 1996). In addition, cisplatin, which is administered intravenously has limited solubility in aqueous solution (Wong and Giandomenico, 1999). Therefore, these have stimulated a search for other transition metal complexes which have higher activity and reduced side-effects.

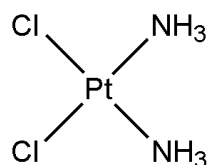


Figure 1.5 Structural formula of cisplatin

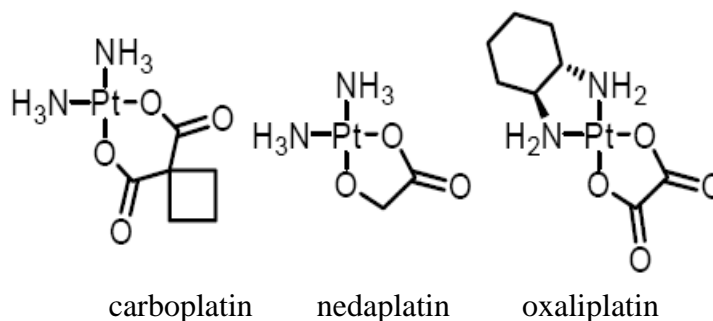


Figure 1.6 Cisplatin analogues used in the clinic

### 1.7 Mechanism of DNA Cleavage

McCord and Fridovich were the first to discover that the enzyme superoxide dismutase is able to dismutate superoxide anion to form oxygen and hydrogen peroxide (McCord and Fridovich, 1969). Transition metal complexes were found can induce DNA cleavage by generating reactive oxygen species (ROS). These ROS have been found to interact directly with DNA or DNA components via singlet oxygen species ( $O_2\bullet$ ) and hydroxyl radicals ( $\bullet OH$ ). One of the methods from which it is produced is the Fenton reaction (Figure 1.7), where a transition metal is oxidised to a higher oxidised state, by donating an electron to a hydrogen peroxide species, resulting in the formation of a hydroxyl radical and a hydroxyl ion.  $\bullet OH$  is one of the most studied reactive biological radicals, and has been implicated in reactions with the nucleic acid bases of DNA.  $\bullet OH$  reacts preferentially with the  $\pi$ -bonds of DNA bases, but can also interact with the sugar units by hydrogen abstraction.  $\bullet OH$  is known to react with each of the four DNA bases, resulting in mutagenic lesions.

While, literature have shown that  $O_2^{\cdot-}$  radicals cannot induce DNA damage (Muller and Burrows, 1998). These  $O_2^{\cdot-}$  can react with  $H^+$  to generate  $H_2O_2$  which in turn can react with more  $O_2^{\cdot-}$  to generate more  $\cdot OH$  via Harber-Weiss reactions.

The  $\cdot OH$  radical will attack the guanine moiety at the C4, C5 or the C8 position. Guanine is the most sensitive base towards oxidative attack. Floyd *et al.* was proving that the major product formed by  $\cdot OH$  and guanine was 8-hydroxyguanine (8-OH-Gua) suggesting that  $\cdot OH$  radicals are involved in the attack of purine bases (Floyd *et al.*, 1986). From Figure 1.8, adduct 1 and 2 revert back to guanine by gaining an electron via thiols generated in the cells. Adduct 3 (8-OH-Gua) can be oxidised to form 8-oxo-Gua and reduced to form formamidopyrimidine (Fapy-G). Cadet *et al.* also implicated the  $\cdot OH$  in tandem DNA base damage (Cadet *et al.*, 1999). This damage via the Fenton reaction can be mediated in vivo by labile transition metals, such as iron (Fe), copper (Cu) and nickel (Ni) (Lloyd and Phillips, 1999).

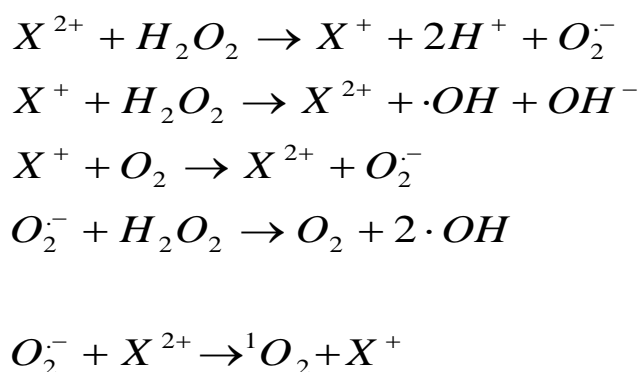


Figure 1.7 Mechanism of Fenton reaction (X represents metal)

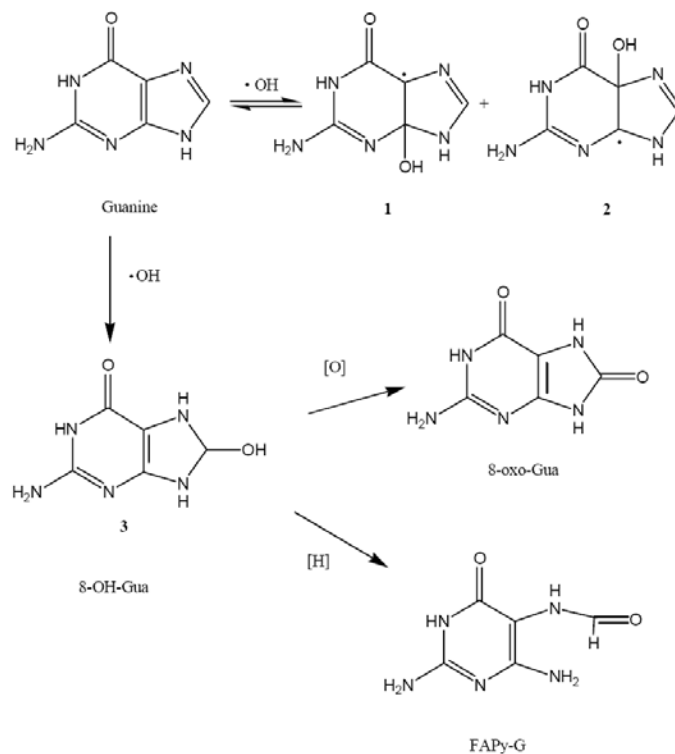


Figure 1.8 Schematic representation for the reaction of guanine with hydroxyl radicals

### 1.8 Biological Activity of Nickel(II) Complexes

Nickel is a compound that occurs in the environment only at very low levels. However, exposure to high levels of nickel pollution has been linked to nasal and lung cancer and nickel is therefore considered a carcinogen (Matkar *et al.*, 2006).

The Occupational Safety and Health Administration (OSHA) has set an enforceable limit of 1.0 mg nickel/m<sup>3</sup> for metallic nickel and nickel compounds in workroom air to protect workers during an 8-hour shift over a 40-hour work week. The Environmental Protection Agency (EPA) recommends that drinking water levels for nickel should not be more than 0.1 mg per liter.

Nickel plays versatile and sometimes controversial roles in living systems (Lancaster, 1998). Biological effects of nickel are closely related to its chemical forms of existence. For example, water-insoluble crystalline Nickel sulfate, NiS and

Nickel(II) oxide, NiO were suspected to induce human lung and nasal cancers (IARC, 1990), while animal studies suggested that water-soluble nickel sulfate did not cause a higher incidence of lung cancer statistically (Dunnick *et al.*, 1995).

As a platinum group metal, nickel(II) may share some similarity with platinum(II). In fact, several nickel complexes have been found to inhibit proliferation of diverse cancer cells (Ferrari *et al.*, 2002; Liang *et al.*, 2004; Matkar *et al.*, 2006). In addition, the ability of certain nickel compounds to interact with DNA and RNA has been exploited for research purposes.

One of the synthetic nickel complexes extensively studied in the past because of its ability to catalyze limited cleavage of nucleic acids contains a ligand known as CR (2,12-dimethyl-3,7,11,17-tetraazabicyclo-[11.3.1]-heptadeca-1(17),2,11,13,15-pentaene).  $[\text{NiCR}]^{2+}$  (Figure 1.9) has been used in the past as a structure-specific probe for RNA and DNA oligonucleotides in the presence of oxidizing agent but little is known about the biological effects of either complex. Matkar *et al.* show that  $[\text{Ni}(\text{CR}-2\text{H})]^{2+}$  can damage DNA in the absence of an added oxidizing agent, oxone (Figure 1.10) and has an  $\text{IC}_{50}$  of 70  $\mu\text{M}$  in human breast cancer cells whereas  $[\text{NiCR}]^{2+}$  and  $\text{NiCl}_2$  do not exhibit significant cytotoxicity (Figure 1.11). However, both  $[\text{NiCR}]^{2+}$  and  $[\text{Ni}(\text{CR}-2\text{H})]^{2+}$  bind to the minor groove of double-stranded DNA (Matkar *et al.*, 2006).

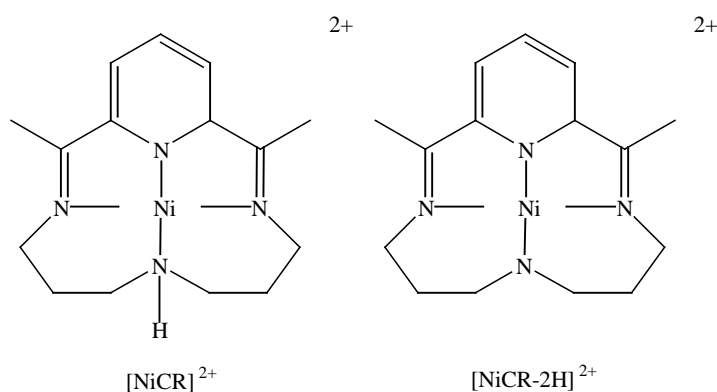


Figure 1.9 The structures of  $[\text{NiCR}]^{2+}$  and  $[\text{Ni}(\text{CR}-2\text{H})]^{2+}$  (Matkar *et al.*, 2006)



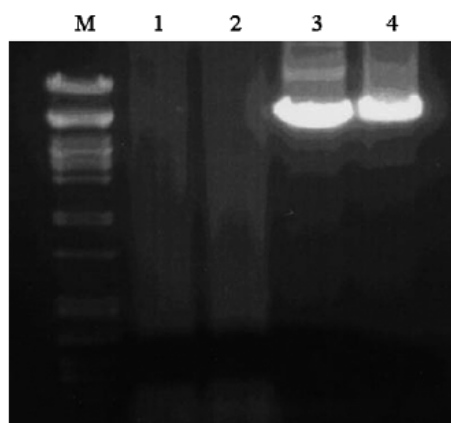


Figure 1.10  $[\text{NiCR}]^{2+}$  and  $[\text{Ni}(\text{CR-2H})]^{2+}$  caused double-stranded DNA damage in vitro in the presence of oxone. The gel shows the DNA samples after piperidine treatment. Lane 1, linearized plasmid DNA treated with  $[\text{NiCR}]^{2+}$  and oxone; lane 2, DNA treated with  $[\text{Ni}(\text{CR-2H})]^{2+}$  and oxone; lane 3, DNA treated with oxone; lane 4, untreated control; M, marker (PstI-cut lambda DNA) (Matkar *et al.*, 2006)

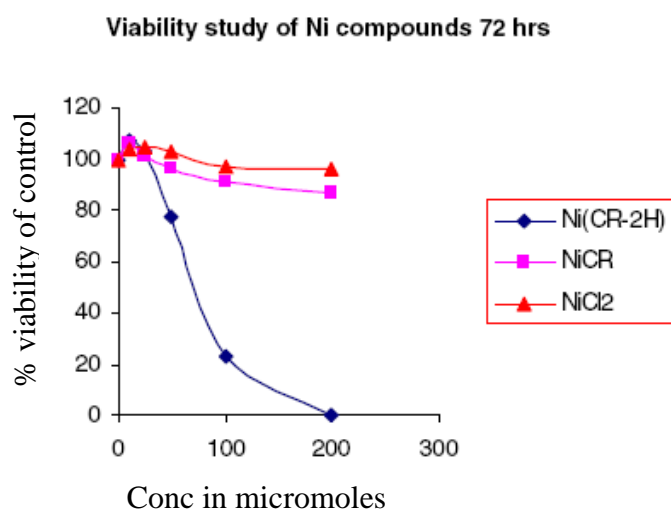


Figure 1.11 Cytotoxicity of  $[\text{Ni}(\text{CR-2H})]^{2+}$ . MCF-7 human breast cancer cells were treated with 10, 25, 50, 100 or 200  $\mu\text{M}$   $\text{NiCl}_2$ ,  $[\text{NiCR}]^{2+}$  or  $[\text{Ni}(\text{CR-2H})]^{2+}$  and cell viability was determined by MTS assay. Diamonds ( $\blacklozenge$ ) stand for  $[\text{Ni}(\text{CR-2H})]^{2+}$ , squares ( $\blacksquare$ ) for  $[\text{NiCR}]^{2+}$ , and triangles ( $\blacktriangle$ ) for  $\text{NiCl}_2$  (Matkar *et al.*, 2006)

Besides, Afrasiabi and partners have also done the research on the nickel(II) complexes of naphthaquinone thiosemicarbazone (NQTS) and semicarbazone (NQSC) (Afrasiabi *et al.*, 2005). These two nickel complexes,  $\text{Ni}(\text{NQTS})_2$  and  $\text{Ni}(\text{NQSC})_2$  were screened in vitro against MCF-7 breast cancer cell lines for their antiproliferation activity.

Figure 1.12 shows the  $IC_{50}$  values ( $\mu M$ ) for the two ligands and their nickel(II) complexes. It is observed that complexation with metal ion in both NQTS and NQSC ligands increases the inhibitory action on MCF-7 cell proliferation. The enhancement of antiproliferation activity by metal complexes can be related to an increase in the lipophilicity so they can penetrate into the cells more easily (Petering *et al.*, 1966). It has also been suggested that metal complexation may be a vehicle for activation of the ligand as the cytotoxic agent (Beraldo *et al.*, 2004).

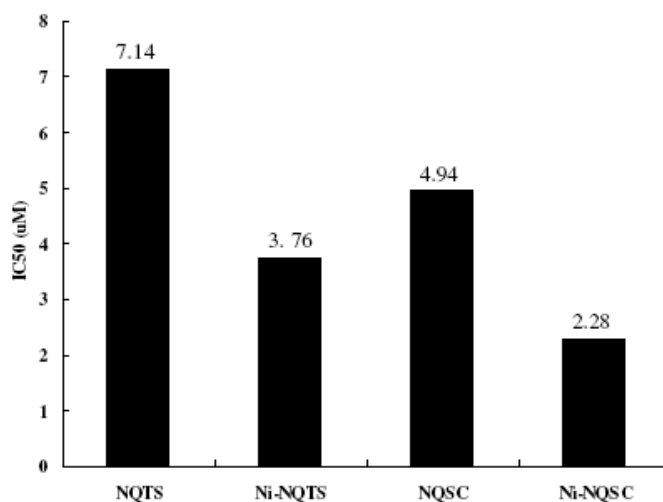


Figure 1.12 Cytotoxic effects of NQTS and NQSC and their nickel(II) complexes on MCF-7 human breast cancer cells (Afrasiabi *et al.*, 2005)

## 1.9 Biological Activity of Iron Complexes

Iron is one of the most important microelements for human health and is known to interact with numerous other dietary components (Lynch, 1997). Iron often exists in the state of complex in the body, which endows it a great deal of physiological function.

Iron is essential to most life forms and to normal human physiology. It is an integral part of many proteins and enzymes that maintain good health. In humans, iron is an essential component of proteins involved in oxygen transport. It is also

essential for the regulation of cell growth and differentiation. A deficiency of iron limits oxygen delivery to cells, resulting in fatigue, poor work performance, and decreased immunity.

Iron in the form of complex may take part in the process of transportation and exchange of the oxygen in blood and also participates in other important metabolism as iron enzyme. However, because  $\text{Fe}^{2+}$  in food has a low biological value it may exchange into the insoluble compounds, which are hard to be adsorbed for its characteristics of being prone to be oxidized and interrupted by oxalate and phosphate (Goldstein and Samuni, 2005). The deficiency of iron micronutrient is one of the most prevalent nutritional problems of humans in developing countries. It has been shown that growing children and women of reproductive age are most vulnerable to the deficiency (Bloem, 1995; Ribaya-Mercado, 1997). Studies show that iron absorption in the body is influenced by several factors, including animal species, dietary factors, i.e. ascorbic acid (Monsen, 1988), pectin content, phytate (Morris and Ellis, 1982), protein sources and amino acids (Martinez-Torres *et al.*, 1981) and the other minerals.

On the other hand, excess amounts of iron can result in toxicity and even death (Corbett, 1995). Excessive iron can be toxic, because free ferrous iron reacts with peroxides to produce free radicals, which are highly reactive and can damage DNA, proteins, lipids, and other cellular components. Thus, iron toxicity occurs when there is free iron in the cell, which generally occurs when iron levels exceed the capacity of transferrin to bind the iron. Humans experience iron toxicity above 20 milligrams of iron for every kilogram of mass, and 60 milligrams per kilogram is a lethal dose. The Dietary Reference Intake (DRI) lists the Tolerable

Upper Intake Level (UL) of iron for adults as 45 mg/day while for children under fourteen years old is 40 mg/day.

El Amrani *et al.* have reported  $[\text{Fe}(\text{3hf})_2\text{Cl}(\text{MeOH})]$  complex as shown in Figure 1.13 for their ability to cleave DNA (El Amrani *et al.*, 2006). As shown in Figure 1.14,  $\text{FeCl}_3$  do not show any DNA cleavage. While at 23  $\mu\text{M}$  of the  $[\text{Fe}(\text{3hf})_2\text{Cl}(\text{MeOH})]$  complex, a mixture of supercoiled plasmid and nicked circular is observed.

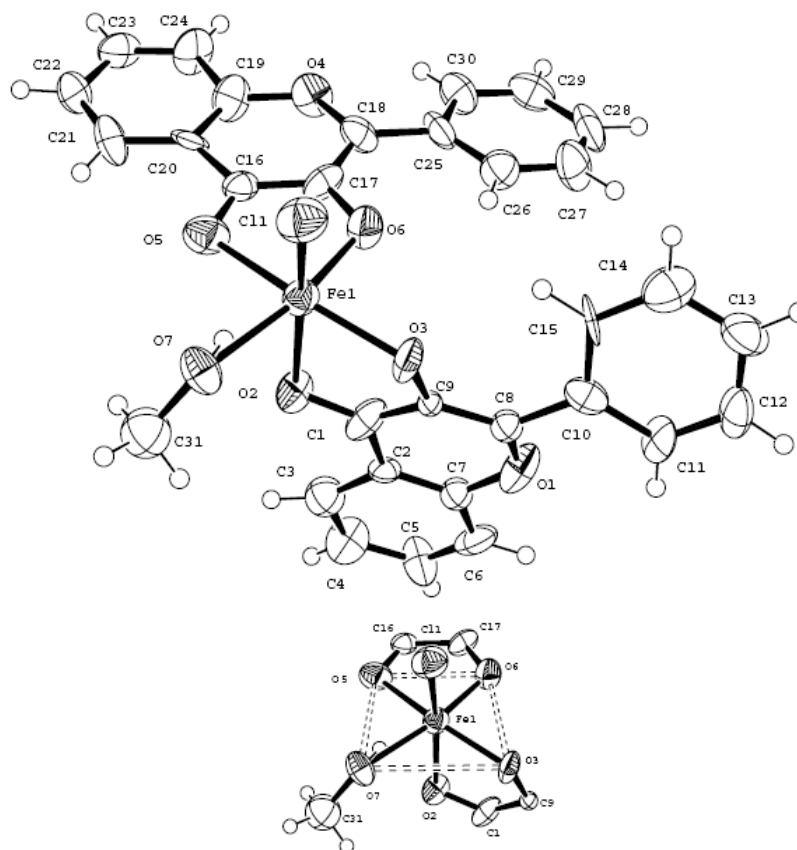


Figure 1.13 ORTEP drawing of the  $[\text{Fe}(\text{3hf})_2\text{Cl}(\text{MeOH})]$  complex (El Amrani *et al.*, 2006)

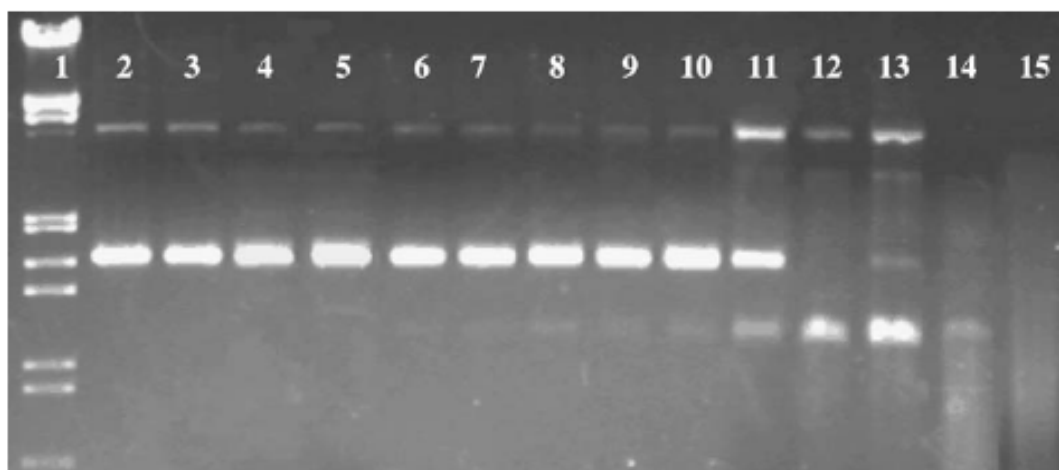


Figure 1.14 Agarose gel electrophoresis of pUC18 plasmid DNA treated with complex,  $\text{FeCl}_3$ , and a mixture  $\text{FeCl}_3 + \text{H3hf}$  (1:2) in the presence of the 1 equiv ascorbate/ $\text{H}_2\text{O}_2$ . Lane 1:  $\lambda\text{DNA}/\text{EcoRI} + \text{HindIII}$  Marker; lane 2: supercoiled DNA; lane 3: supercoiled DNA + ascorbate/ $\text{H}_2\text{O}_2$ ; lane 4:  $15 \mu\text{M}$   $\text{FeCl}_3$ ; lane 5:  $21 \mu\text{M}$   $\text{FeCl}_3$ ; lane 6:  $27 \mu\text{M}$   $\text{FeCl}_3$ ; lane 7:  $27 \mu\text{M}$   $\text{FeCl}_3 + 54 \mu\text{M}$   $\text{H3hf}$ ; lane 8:  $15 \mu\text{M}$  complex; lane 9:  $18 \mu\text{M}$  complex; lane 10:  $21 \mu\text{M}$  complex; lane 11:  $23 \mu\text{M}$  complex; lane 12:  $25 \mu\text{M}$  complex; lane 13:  $26 \mu\text{M}$  complex; lane 14:  $27 \mu\text{M}$  complex; lane 15:  $30 \mu\text{M}$  complex (El Amrani *et al.*, 2006)

Besides, Travnicek and coworkers have tested iron complexes involving N6-benzyladenosine derivatives (L1–L7) of the predominant composition  $[\text{Fe}(\text{L})\text{Cl}_3] \cdot \text{H}_2\text{O}$  for their in vitro cytotoxicity against human cancer cell lines of malignant melanoma (G-361), osteogenic sarcoma (HOS), chronic myelogenous leukemia (K-562), and breast adenocarcinoma (MCF-7) (Travnicek *et al.*, 2008). All free N6-(benzylamino)adenosine derivatives (L1–L7), used as ligands, showed cytotoxicity with  $\text{IC}_{50} > 50 \mu\text{M}$ , and  $\text{FeCl}_3 \cdot 6\text{H}_2\text{O}$  even above  $200 \mu\text{M}$ . The results of selected  $\text{IC}_{50}$  values is shown in Table 1.1. From the results, complex 2,  $[\text{Fe}(\text{L}_2)\text{Cl}_3] \cdot \text{H}_2\text{O}$  showed significant cytotoxicity against the HOS, K-562, and MCF-7 cell lines, respectively. Moreover, a considerable cytotoxicity has been found for the complex 6,  $[\text{Fe}(\text{L}_6)\text{Cl}_3] \cdot \text{H}_2\text{O}$  on the MCF-7 cell line.

Table 1.1 Selected IC<sub>50</sub> (μM) values assessed by a calcein AM assay (Travnicek *et al.*, 2008)

Compound	IC <sub>50</sub> (μM)			
	G-361	HOS	K-562	MCF-7
[Fe(L <sub>2</sub> )Cl <sub>3</sub> ] · H <sub>2</sub> O (2)	>50	8	9	16
L <sub>2</sub>	>50	>50	>50	>50
[Fe(L <sub>6</sub> )Cl <sub>3</sub> ] · H <sub>2</sub> O (6)	>50	>50	>50	4
L <sub>6</sub>	>50	>50	>50	>50
FeCl <sub>3</sub> ·6H <sub>2</sub> O	>200	>200	>200	>200

L<sub>2</sub>=N6-(4-fluorobenzyl)adenosine; L<sub>6</sub>=N6-(4-trifluoromethoxybenzyl)adenosine. The human cancer cell lines (G-361, malignant melanoma; HOS, osteogenic sarcoma; K-562, chronic myelogenous leukemia; MCF-7, breast adenocarcinoma) were treated with the solution of the tested compound in the 0.5-50 μM range for 72 h, except for FeCl<sub>3</sub>·6H<sub>2</sub>O, where the concentration range of 0.5-200 μM was used.

### 1.10 Objectives and Scope of Study

The objectives of this research is to synthesize a series of complexes formed by the reaction of carboxylic acids with nickel(II) chloride hexahydrate, NiCl<sub>2</sub>·6H<sub>2</sub>O, iron(II) chloride 4-hydrate, FeCl<sub>2</sub>·4H<sub>2</sub>O and ferric chloride anhydrous, FeCl<sub>3</sub> respectively. The acids utilised were amino acid, carboxylic acid and dicarboxylic acid derivatives and are listed in Table 1.2.

Table 1.2 Carboxylic acids utilised in this study

Acids	Name
Amino acid derivatives	Glycine; β-alanine; L-histidine.
Carboxylic acid derivatives	2-picolinic acid; 3,5-dinitrobenzoic acid; 4-aminobenzoic acid; pyrazine-2-carboxylic acid.
Dicarboxylic acid derivatives	Maleic acid; pyridine-2,6-dicarboxylic acid

The complexes that are successfully synthesized will be characterized by determination of melting point, solubility, conductivity measurement, elemental microanalysis (C, H, N), Atomic Absorption Spectrometry (AAS), Fourier

Transform Infrared Spectroscopy (FTIR), Ultraviolet-Visible Spectrometry (UV-Vis), Cyclic Voltammetry (CV) and X-ray crystallography.

Besides that, the interaction between the metal complexes and pBR322 DNA will be investigated by gel electrophoresis experiments, while the cytotoxic activity of the complexes will be tested against human hepatoma cell line (HepG2).

## CHAPTER 2

### MATERIALS AND METHODS

#### 2.1 Reagents

Table 2.1 and Table 2.2 show the features and the suppliers for all the chemicals and biochemicals which were used in this research. All of these chemicals were used without further purification.

Table 2.1 Chemicals used in this research

Chemicals	Molecular Weight (g/mol)	Purity (%)	Supplier
Nickel(II) chloride hexahydrate NiCl <sub>2</sub> .6H <sub>2</sub> O	237.70	97%	Riedel-deHaen
Iron(II) chloride 4-hydrate FeCl <sub>2</sub> .4H <sub>2</sub> O	198.81	98%	BDH Chemicals Ltd.
Ferric chloride anhydrous FeCl <sub>3</sub>	162.21	98%	GCE Laboratory Chemicals
Glycine C <sub>2</sub> H <sub>5</sub> NO <sub>2</sub>	75.07	100.11%	Fisher Chemicals
β-alanine C <sub>3</sub> H <sub>7</sub> NO <sub>2</sub>	89.09	≥ 99%	Fluka Chemika
L-histidine C <sub>6</sub> H <sub>9</sub> N <sub>3</sub> O <sub>2</sub>	155.16	99%	BDH Chemicals
2-picolinic acid C <sub>6</sub> H <sub>5</sub> NO <sub>2</sub>	123.11	98%	Fluka Chemika
Pyrazine-2-carboxylic acid C <sub>5</sub> H <sub>4</sub> N <sub>2</sub> O <sub>2</sub>	124.10	99%	Aldrich
3,5-dinitrobenzoic acid C <sub>7</sub> H <sub>4</sub> O <sub>6</sub> N <sub>2</sub>	212.12	99.5%	BDH Chemicals Ltd.
4-aminobenzoic acid C <sub>7</sub> H <sub>7</sub> NO <sub>2</sub>	137.14	99.5%	G.P.R
Maleic acid C <sub>4</sub> H <sub>4</sub> O <sub>4</sub>	116.08	≥ 99%	Fluka Chemika
Pyridine-2,6-dicarboxylic acid C <sub>7</sub> H <sub>5</sub> NO <sub>4</sub>	167.12	≥ 98%	Fluka Chemika
Potassium Hydroxide KOH	56.11	85%	System
Sodium Hydroxide NaOH	40.00	99%	System
Nitric Acid HNO <sub>3</sub>	63.01	65%	System



Table 2.2 Biochemicals used in biology part

<b>Biochemicals</b>	<b>Supplier</b>
pBR322 DNA	Fermentas
GeneRuler 1kb DNA Ladder	Fermentas
6X Loading Dye Solution	Fermentas
1X TAE buffer	BIO-RAD Laboratories
Tris-HCl	AMRESCO
DMSO	Fluka Chemika
Tert-butanol	QReC
D-mannitol	R & M Chemicals
Potassium Iodide, KI	Fisher Scientific
Hydrogen Peroxide, H <sub>2</sub> O <sub>2</sub>	Fluka Chemika
Sodium Azide, NaN <sub>3</sub>	Fisher Scientific
Ethidium Bromide, EtBr	Fluka BioChemika
HepG2	ATCC, Manassas, VA, USA
Eagle's Minimum Essential Medium, MEM	Invitrogen (GIBCO), USA
Fetal Bovine Serum, FBS	Invitrogen (GIBCO), USA
Phosphate Buffered Saline, PBS	Invitrogen (GIBCO), USA
Trypsin	Invitrogen (GIBCO), USA
MTT	Invitrogen (GIBCO), USA
Penicillin	Invitrogen (GIBCO), USA
Streptomycin	Invitrogen (GIBCO), USA

## 2.2 Instrumentation

The instrumentation used for the quantitative and qualitative characterization of the carboxylate complexes are listed in Table 2.3.

Table 2.3 Instruments used for the quantitative and qualitative characterizations

<b>Instruments</b>	<b>Model</b>
Melting Point Apparatus	Gallenkamp Variable Heater
Conductivity Measurement	CyberScan 500 instrument
FT-IR Spectrophotometer	Perkin-Elmer System 2000
Elemental Analyzer (CHNS/O)	Perkin-Elmer Series II 2400
Atomic Absorption Spectroscopy	Perkin-Elmer AAS model 3100
Ultraviolet-Visible (UV-Vis) Spectrometry	Model Jasco V-530
Cyclic Voltammetry (CV)	BAS Epsilon EC-20
Thermogravimetric Analysis (TGA)	Mettler Toledo TGA/SDTA851e
X-Ray Crystallography	Bruker SMART APEX2 CCD

### **2.3 Experimental**

Nickel(II) chloride hexahydrate was used as the starting material to prepare the complex. The molar ratio of starting material:ligand was in 1:2 ratio in the synthesis of the complexes. Nickel(II) chloride hexahydrate (1 g, 4.2070 mmol) was dissolved in 30 mL of distilled water. The green solution was put into a two-neck round flask. All the ligands were dissolved in 30 mL of distilled water before mixed into the two-neck round flask. Then the mixture was refluxed with constant stirring over an oil bath at 80 °C for 3 hours. In alkaline condition, the pH of the mixture was adjusted to pH 8 with 2M KOH before heating it under reflux. After that, the solution was filtered while it was still hot. Then the filtrate was left to evaporate to dryness at room temperature. The crystals were obtained after a few days of evaporation. The synthesis methods for the complexes of iron(II) chloride 4-hydrate(1 g, 5.0299 mmol) and ferric chloride anhydrous (1 g, 6.1648 mmol) were same as the method above.

### **2.4 Methods of Characterization**

All the characterization analysis had been done in School of Chemical Sciences, Universiti Sains Malaysia.

#### **2.4.1 Determination of the melting point of complexes**

Melting point for each complex was determined using Gallenkamp Variable Heater in a capillary tube. The complex was observed through a window of the heater. The temperature was recorded when it was melted.

#### **2.4.2 Conductivity Measurement**

The complexes were dissolved in warm distilled water. The measurement was conducted on molarity  $10^{-3}$  M of every complex solution by using CyberScan 500 instrument.

#### **2.4.3 Analysis of Fourier Transform Infrared Spectroscopy (FT-IR)**

The infrared spectra of the complexes were obtained by using Perkin-Elmer System 2000 in the region of  $4000-400\text{ cm}^{-1}$  at room temperature.

Every dry analyte (complexes, ligands and salts of the ligands) was ground with potassium bromide (KBr) in the ratio of 1:10 to obtain fine and evenly ground powder. The fine powder was then pressed into pellets at 7 tonne of pressure by vacuum pump. Spectra were recorded from  $400$  to  $4000\text{ cm}^{-1}$ .

#### **2.4.4 CHN Microanalysis**

Microanalysis for the elements of carbon, hydrogen and nitrogen were carried out by using CHNS/O Analyzer (Perkin-Elmer Series II 2400).

#### **2.4.5 Analysis of Atomic Absorption Spectrometry (AAS)**

This analysis was conducted to determine the nickel and iron content in each complex. It was carried out on a Perkin-Elmer Atomic Absorption Spectroscopy model 3100. The preparation of standard solution and sample solution was described as below:

1) Preparation of standard solution

The stock solution of nickel and iron were prepared from 1000 ppm of standard solution. While the stock solution of potassium was prepared from 10 ppm

of standard solution. Stock solution was pipetted to a 100 mL volumetric flask by using micropipette. Then the solution was diluted to 100 mL by using 2 % of nitric acid.

A series of nickel, iron and potassium standard solution were prepared in the range of 1-5 ppm. The calibration curve for their total content was constructed based on the absorbances that were exhibited by a series of standard solutions as in Appendix. The calibration curve for nickel, iron and potassium are depicted in Figure 2.1, Figure 2.2 and Figure 2.3 respectively.

## 2) Preparation of sample solution

The stock solution of nickel complexes were prepared by dissolved 0.02 g of complex in 15 mL of concentrated nitric acid and diluted to 100 mL in 100 mL volumetric flask by using 2% of acid nitric. After that, 10 mL was pipetted from the volumetric flask into a 100 mL volumetric flask and diluted to 100 mL with 2% of nitric acid. The preparation for stock solution of iron complexes was the same as nickel.

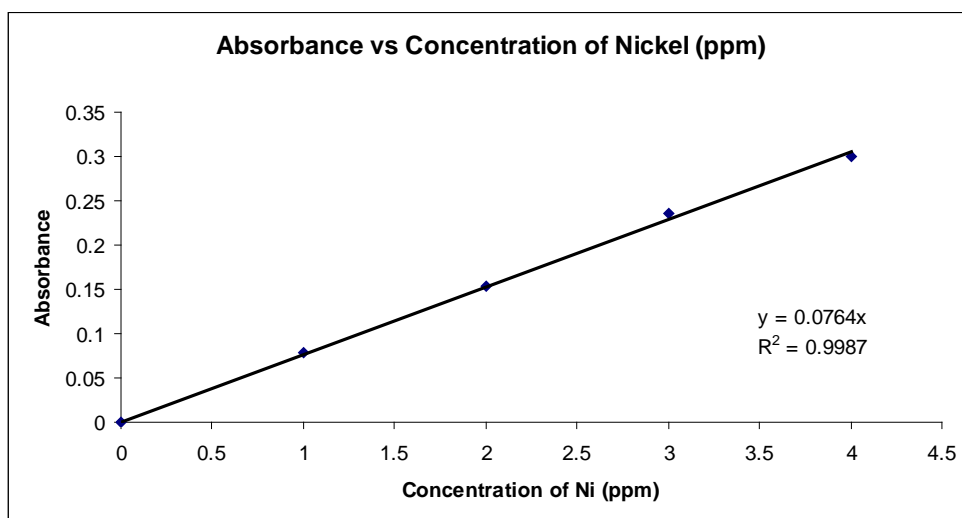


Figure 2.1 The AAS calibration curve for nickel

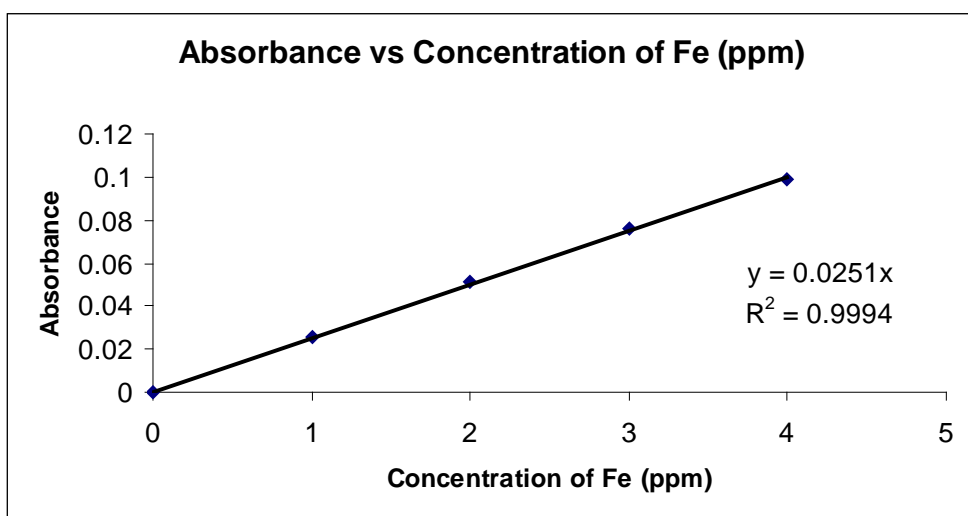


Figure 2.2 The AAS calibration curve for iron

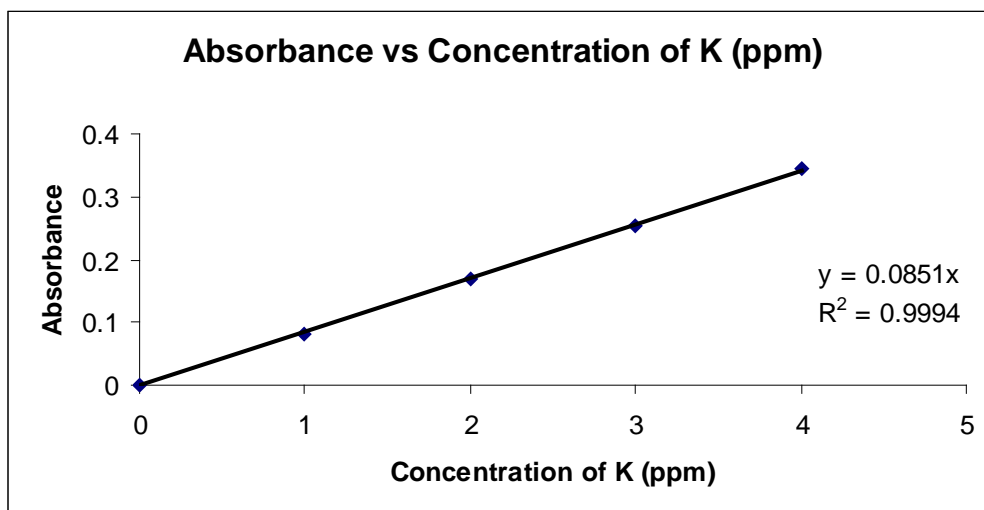


Figure 2.3 The AAS calibration curve for potassium

#### 2.4.6 Analysis of Ultraviolet-Visible (UV-Vis) Spectrometry

UV-Visible spectra were measured using Model Jasco V-530. Approximately 0.03 g of sample was dissolved in distilled water. Dilution process was carried out to obtain clear spectra. The measurement wavelength was set in the range of 200-1000 nm.